

Carbon Nanomaterials for Emerging Electronic Devices and Sensors



Venkatarao Selamneni, Naveen Bokka, Vivek Adep, and Parikshit Sahatiya

Abstract Over the last two decades, carbon nanomaterials including two-dimensional graphene, one-dimensional carbon nanotubes (CNTs), and zero-dimensional carbon quantum dots, fullerenes have gained tremendous attention from researchers due to their unique optical, electronic, mechanical, chemical, and thermal properties. Furthermore, to enhance the properties of pristine carbon nanomaterials, their hybrid materials have been synthesized. Even though tremendous advancement in carbon nanomaterials-based electronic devices and sensors has been achieved, a few challenges need to be addressed before the commercialization of carbon nanomaterials-based devices. Apart from the improvements, the device to device variations, and extrinsic factors like dielectric layers, metal contact resistance remain an issue. Strategies such as chemically tuning and enhancing the properties of carbon nanomaterials are important for the further improvement of carbon nanomaterial-based device performance. This chapter focuses on understanding the basic electronic properties of graphene, CNT, and carbon quantum dots/fullerenes and their applications in electronic devices (field-effect transistors, diodes, etc.), optoelectronics, and various chemical and physical sensors.

Keywords Carbon nanomaterials · Fullerenes · Carbon quantum dots · Carbon nanotubes · Graphene · CNTFET · GFET · Chemical sensors · Physical sensors · Photodetectors

1 Introduction

Solid materials with at least one dimension restricted to the nanoscale (1–100 nm) are called nanomaterials. Materials whose size range in micro-meter have their properties almost similar to that of the bulk materials, but on the other hand, nanomaterials have unique and different properties such as higher surface to volume ratio,

V. Selamneni · N. Bokka · V. Adep · P. Sahatiya (✉)
Department of Electrical and Electronics Engineering, Birla Institute of Technology and Science
Pilani Hyderabad Campus, Hyderabad 500078, India
e-mail: parikshit@hyderabad.bits-pilani.ac.in

© The Author(s), under exclusive license to Springer Nature Singapore Pte Ltd. 2021
A. Hazra and R. Goswami (eds.), *Carbon Nanomaterial Electronics: Devices and Applications*, Advances in Sustainability Science and Technology,
https://doi.org/10.1007/978-981-16-1052-3_10

215

improved electrical, thermal, mechanical, optical properties, and with minimal imperfections which are completely diverse from bulk counterparts. In 1985 first carbon material named buckminsterfullerene (C_{60}) was synthesized and then later, various other carbon materials came into existence. Over the years, carbon nanomaterials such as fullerenes, nanodiamonds, nanotubes, nanofibers, and graphene have got the utmost prominence for their utilization in various applications. We must understand these different carbon nanomaterials before a detailed discussion regarding different applications.

1.1 Fullerene

Carbon atoms organized in hexagonal and pentagonal rings with closed hollow cages are known as fullerenes. Cylindrical/ ellipsoidal, the spherical arrangement of molecules that entirely contain carbon atoms falls under the category of fullerenes. Carbon nanotubes/bucky tubes are cylindrical-shaped fullerenes, and spherical-shaped fullerene is known as buckyballs.

Spherical Fullerene

This class of carbon materials is zero-dimensional in which all the dimensions of the molecule are restricted to the nanoscale. C_n is the chemical formula of the spherical fullerene where the number of carbon atoms existing in a fullerene molecule is denoted by n in C_n . These are classified into C_{60} , C_{70} , C_{76} , C_{84} , and this sequence continues till gigantic [1] (where the number of carbon atoms greater than 100) and fullerenes of onion type [2] (where concentric shells are combined to form a hollow shape structure). Among all the fullerene structures, buckminsterfullerene- C_{60} is the most stable and prominent structure. It is the carbon molecule in which pentagonal faces are out-of-the-way with each other with a diameter of approximately 0.683 nm. Fullerenes are found as less stable dynamically but considered as chemically more stable in comparison to graphite. These are applied in various applications such as photodetectors [3], solar cells [4], field-effect transistors [5], etc (Fig. 1).

1.1.1 Carbon Nanotubes

Carbon atoms of sp^2 hybridization must be bent to form fullerenes of cylindrical structures known as carbon nanotubes. During the thermal decomposition of various hydrocarbons, it was found that there is a possibility of the formation of carbon filaments before the invention of a transmission electron microscope (TEM) [6]. Later after the invention of TEM, it is confirmed that tubular structures like that of nanotubes came into existence from various reports issued in the twentieth century. The carbon filaments of nano size and tubular form using TEM images in 1952 were stated by Radushkevich and Lukyanovich [7]. The first CNT was grown without the usage of any catalyst in a report published by Iijima in 1991 [8]. Different methods

such as chemical vapor deposition [9, 10], laser ablation [11], arc discharge [12], etc., are employed for the production of CNTs. CNTs have an analogous structure as that of three-Dimensional graphite because it is derived from the rolled monolayer layer of graphite structure. If the tube wall of carbon nanotube is formed from only one-layer, multiple layers of graphite, then they are known as SWCNTs (single-walled carbon nanotube) and MWCNTs (multi-walled carbon nanotubes), respectively. Intertube spacing in MWCNTs is 0.34 nm almost similar to that of the interlayer distance between carbon atoms of graphite structure [13]. In CNTs, only one dimension of the structure is restricted to the nanoscale, therefore it is considered as a one-dimensional nanomaterial with several hundred nanometers of diameter [14] and length up to several centimeters [15]. Chiral vector (C_h) represents the structure of the SWCNTs. Two integers (n,m) and base vectors a_1 , a_2 will define the chiral vector of the CNTs [16, 17]. These integers of chiral vector classify SWCNTs into the armchair tubes (when $m = n$ i.e., (n, n)), zig-zag tubes (when $m = 0$, i.e., $(n, 0)$) and for other possible (n, m) values of integers, they are chiral tubes. The information about the chiral angle and the diameter of the nanotubes is known by integer indices (n, m) [18]. The electrical properties of SWCNTs are proportionate to the chirality of nanotubes. When $m-n/3$ is an integer then nanotube (SWCNT) is considered as metallic or else for all other conditions it is a semiconductor. From various reports, it is confirmed that CNTs are unique carbon nanomaterials with improved electrical, thermal, mechanical, and various other properties for utilizing them in different applications such as flat panel displays [19], sensing devices [20, 21], Li-ion batteries [22], fuel cells [23, 24], etc (Fig. 2).

1.2 Carbon Nanofibers

Carbon nanofibers are a different class of carbon nanomaterial in which the filament-like structure of graphite completely different from nanotubes is aligned in the monolayer graphitic planes. Nanofibers are those in which layers of graphite are organized at an angle (herringbone form) or perpendicular to the plane (stacked form) of the fiber axis [27]. Subjecting hydrocarbons in gaseous form to high temperatures in the presence of catalyst will result in carbon nanofibers. Factors influencing the carbon nanofibers are catalyst material, the temperature used for the synthesis, reactant gas composition. These carbon nanofibers have exceptional mechanical properties such as high mechanical strength which is used in nanocomposite preparation for various applications [28] (Fig. 3).

1.3 Graphene

Graphene is a two-dimensional carbon nanomaterial that is formed from single or various monolayers of graphite. Carbon atoms of sp^2 hybridization are tightly

crammed with a bond length of 0.142 nm, in a honeycomb crystal lattice. An only sheet of graphene is termed single-layer graphene (SLG) and multiple sheets superimposed upon one another with an interplanar spacing of 0.335 nm are called few-layered graphene (FLG). Graphene is considered a basic building block of carbon nanomaterials. Zero-dimensional (spherical fullerene) and one-dimensional (nanotubes) carbon nanomaterial can be easily prepared from graphene by wrapping layers in a specific direction of the material. During 1990 and 2004, using the mechanical exfoliation technique several attempts are made for producing thin films of graphite which resulted in the making of nothing less than numerous tens of layers [30]. In 2004, Novoselov and Geim succeeded in the production of graphene in the order of single-atom thickness from bulk graphite structure using a technique known as the micro-mechanical cleavage [31]. Most of the reported methods such as mechanical exfoliation [31], chemical vapor deposition [32], oxidation of graphite [33], liquid-phase exfoliation [34], etc., have challenges in controlling the size, shape, and other parameters during the synthesis of graphene. Apart from all these hardships in synthesis, still, graphene has been utilized in different applications owing to its remarkable mechanical, thermal, electrical, and other properties [35–38] (Fig. 4).

Different properties of the above-discussed carbon-based nanomaterials such as electrical, elastic, mechanical, etc., are shown in Table 1.

1.4 Carbon Quantum-Dots

A quantum dot is a zero-dimensional nanomaterial relative to bulk materials. It is a fluorescent semiconducting nanocrystal that consists of elements from the periodic table from II to VI, III to V, or IV to VI groups (e.g., CdTe) [40]. The size of these nanomaterials is in the range of 2–10 nm in diameter and contain 200–10,000 atoms approximately [41]. Quantum dots are highly photostable due to the quantum confinement effect with broad absorption, symmetric, and narrow emission spectra. Size, surface chemistry, and chemical composition of nanomaterials are important for the emitted light and can be adjusted to visible and near-infrared regions from the UV region. Electron energy levels of the bulk form of semi-conductor are continuous and these energy levels are distinct due to the quantum confinement effect at the nanoscale. Coulomb stated that electron–hole pair is created due to jumping off an electron from the valency band to the conduction band as exciton and physical confinement of electrons in 3D leads to quantum confinement [42, 43]. An electron that is vaulted into the CB (conduction band) will fall back to the VB (valence band) resulting in radiation (electromagnetic) which is diverse in comparison to actual inducement. The frequency with which it is emitted is allegedly attributed to fluorescence which depends on the size of the bandgap that can be tuned by altering the size and surface chemistry of the quantum dot. Therefore, it is concluded that the smaller the quantum dot higher will be its bandgap.

Table 1 Properties of carbon-based nanomaterials. Reprinted with permission from [39]. Copyright © 2017 Elsevier Ltd. All rights reserved

Property	Fullerene	Single-wall carbon nanotube (SWCNT)	Double-wall carbon nanotube (DWCNT)	Multi-wall carbon nanotube (MWCNT)	Graphene	Carbon-based nanofiber
Density (g/cm ³)	1.7	1.3–1.5	1.5	1.8–2.0	N.A	2.25
Electrical conductivity (S/m)	10 ⁻³	10 ⁶	10 ⁶	10 ⁶	6 × 10 ⁵	10 ³
Distinctive diameter (nm)	0.7	1	5	20	N.A	50–500
Tensile strength (GPa)	N.A	50–500	23–63	10–60	130	3–7
Thermal conductivity in ambient temperature conditions (W/m-K)	0.4	6000	3000	2000	5000	1900
Elongation at break (%)	N.A	5.8	28	N.A	20	05–2.5
Thermal solidity (in the air)	600	>700	>700	>700	450–650	N.A
Specific surface area (m ² /g)	42–85	10–20	10–20	10–20	2675	50
Elastic modulus (TPa)	N.A	1	N.A	0.3–1	1	0.5

NA—Not Available

Carbon-based quantum dots are a class of this zero-dimensional nanomaterial that consists of graphene quantum dots and carbon-quantum dots with a size of less than 10 nm. Carbon-based quantum dots because of their durable luminescence and admirable solubility have got great attention to be called carbon-based nano lights [43, 44]. They are synthesized using various methods such as laser ablation [45], chemical ablation [46, 47], electrochemical carbonization [48, 49], hydrothermal/solvothermal [50, 51], etc. These types of quantum dots have exceptional electronic properties which lead to chemiluminescence and electro-luminescence made potential applications in sensors, photodetectors, catalysis, etc. Over the years, 0D, 1D, 2D carbon nanomaterials (Fullerene, nanotubes, graphene) have got a wide range of scope due

to their exceptional electronic, thermal, optical, chemical, and mechanical properties [52]. Electronic devices such as CNTFET, RF transistors fabricated using graphene, CNT-based digital logic circuits, etc., have improved their performance due to usage of carbon-nanomaterials during their device fabrication. Various physical and chemical sensors such as pressure sensors, strain sensors, electrochemical, biosensors, humidity sensors, etc., have improved their sensing properties by using pristine as well as hybrid carbon nanomaterials. In this chapter, a brief description of pristine, hybrid carbon nanomaterials applications in different electronic, optoelectronic, and sensing devices is discussed.

2 Carbon Nanomaterials-Based Electronic Devices

The exploitation of carbon nanomaterials as electronic materials with high mobility is done due to the extreme delocalization of its sp^2 hybridized electronic structure. Furthermore, in semiconducting CNTs bandgap and diameter are dependent on its atom arrangement called chirality. Therefore, the tunable bandgap of CNTs offers unique opportunities to customize optoelectronic properties. In comparison to conventional semiconducting materials, carbon nanomaterials are found as probable replacements in various electronic applications based on the above reasons [53]. This section provides recent developments in carbon nanomaterials-based electronic devices.

2.1 CNTs Materials in Digital Electronics Applications

In field-effect transistors, semiconducting CNTs are used as capable materials for the channel. If current flows using a channel that is made of CNT material which is in between the drain and source terminals of the FET device, then it is called CNTFET which has three terminals (Fig. 5a). In 1991, the MWCNT was the first CNT to be discovered; but after 2 years, SWCNT was synthesized by researchers [8]. The research on the development of CNT FETs using SWCNTs was increased significantly compared to MWCNTs due to its better tunability of bandgap. CNTFETs are classified into four types: (1) Conventional CNTFETs, (2) Schottky barrier CNTFETs, (3) Tunnel CNTFETs, and (4) Partially gated CNTFETs. In conventional CNTFETs, doped CNT is used as a channel that is similar to the conventional MOSFETs. Undoped CNTs are used in the Schottky barrier CNTFETs which creates the Schottky barrier with metals at source and drain. Tunnel CNTFETs consist of oppositely doped drain and source regions, and partially gated CNTFETs of partial gate region covering channel. Minimal parasitic capacitances, small switching energies are observed due to smaller value of capacitance (i.e. < 0.05 aF/nm) of CNTs and atomically smooth surface of CNTs decreases the carriers scattering and scattering at small-angle carriers which outcomes in only onward and backward scattering are

removed by the 1D structure of CNTs [54, 55]. In comparison to other semiconductors with high mobility, for example, InSb, CNTs have shown high minimal field mobility of greater than $100,000 \text{ cm}^2/\text{Vs}$ and current densities of 10^8 A/cm^2 at room temperature conditions [56, 57]. Also, CNTs have few limitations in nanoelectronic applications, particularly the contact resistance between one-dimensional CNT and metal electrodes has a lower limit of $\sim 6.45 \text{ k}\Omega$ [58]. Further, the contact resistance increases due to the Schottky contacts between CNTs and metals. The difference in CNT Fermi level and metalwork function can be accustomed to allow both FETs of p-type and n-type due to the ambipolar nature of CNTFETs intrinsically. Without tuning of electrode work function or internal doping, generally, CNTFETs are p-type in ambient conditions due to oxidation [59, 60].

The first CNT FET was demonstrated in 1998 (Fig. 5b) [61]. These Initial studies sparked substantial interest in transport phenomena and electronic devices based on CNTs for example SET(single-electron transistors) and wired like structures at the quantum level (quantum wires) [62], ballistic transistors [63], Luttinger liquid behavior [64], and ambipolar FETs [65]. In the early research, Snow et al. studied the transport properties of fabricated thin film transistor s(TFT) using as-grown random CNTs [66]. The on/off ratio of 10^5 and field-effect mobility of $10 \text{ cm}^2/\text{Vs}$: are seen in CNT-based TFTs. The study revealed the trade-offs between field-effect mobility and on–off ratio. From the simulation studies, it was deep-rooted that percolation effects dominate the transport of charge in CNT FETs. Percolation effect displayed power-law relation channel resistance with channel width and length, CNT alignment, CNTs network density. Due to two reasons, CNT TFTs field-effect mobility (i.e., $<100 \text{ cm}^2/\text{Vs}$) is found lower than that of SWCNT (i.e. $>10,000 \text{ cm}^2/\text{Vs}$). First, contact resistance of CNT-CNT in percolating network [67]. The second reason being the overestimation of the random network CNTs capacitance. Numerical methods were used to suppress the consequence of metallic CNTs for overcoming the on/off ratio of digital circuits. Collins et al. reported a selective removal of metallic CNTs using Joule heating [68]. This technique is successful particularly for CNTs which are grown using the CVD method, where all CNTs bridge the drain and source gap. The drawback of this technique is, it causes collateral damage to adjacent nanotubes.

DGU (Density gradient ultracentrifugation) centrifuged semiconducting CNT inks-based devices showed larger values of on/off ratios, current densities, field-effect mobilities [69]. Simple assembly methods such as transfer printing, dip coating, and drop-casting mostly use these semiconducting CNT inks. The density of these semiconducting CNTs could be improved without affecting the on–off ratio. Apart from DGU-sorted CNTs, methods that are based on gels also showed a higher value of on/off ratio which is greater than 10^4 [70]. Roberts et al. fabricated low-voltage TFTs with semiconducting CNTs, with effective device mobility of $13.4 \text{ cm}^2/\text{Vs}$, on/off ratio of >1000 , and a low subthreshold swing (130 mV/dec) [71] (Fig. 5).

2.2 Carbon Nanotubes for Radiofrequency Transistors

Due to high saturation velocity and carrier mobility, the low intrinsic capacitance of CNTs, they have been significantly used as a material for the channel which is used to fabricate high-performance radio-frequency (RF) transistors [73]. CNT-based RF transistors showed extraordinary linearity that is desirable in RF devices. Steiner et al. with the help of aligned semiconducting CNTs fabricated a radio frequency transistor. For a 100 nm gate length, power gain cut-off frequency of 7 GHz (153 GHz, intrinsically) and current gain cut-off frequencies of 15 GHz (30 GHz, intrinsically) output current was saturated [74]. Cao et al. studied the RF performance of fabricated CNT transistors based on high-density, aligned, polyfluorene-sorted semiconducting CNTs with a self-aligned T-shaped gate (Fig. 6) [75]. The fabricated RF transistor exhibited excellent DC with transconductance of $310 \mu\text{S}/\mu\text{m}$, output normalized resistance $>100 \text{ k}\Omega \cdot \mu\text{m}$, and both current gain cut-off frequency and oscillation frequency were greater than 70 GHz. Further, the transistor displayed good linearity with 22 dBm of third-order intercept point (IIP3) and 14 dBm of $P_{1\text{dB}}$ (gain compression point). Zhong et al. demonstrated an RF transistor depends on arbitrarily oriented semiconducting CNT films [76]. The maximum transconductance of $0.38 \text{ mS}/\mu\text{m}$ was achieved by reducing the CNT/CNT junctions and at 103 GHz (281 GHz, intrinsically) current gain cut-off frequency, up to 107 GHz (190 GHz, intrinsically) power gain cut-off frequency.

2.3 Graphene for Digital Electronics

Graphene has been used to explore its applications in digital electronics due to its remarkable field-effect mobility [77]. The better scaling of the device channel is permitted due to its two-dimensional structure [78]. Unlike CNTs, the device's high conductance is attributed to their lower values of contact resistance. But, very low on-off ratio (5–10) and due to the presence of zero bandgap in graphene, it is not used for applications such as digital electronics wherein the anticipated on/off ratio is very high (i.e., in the range of 10^4 – 10^6). Even at zero carrier concentration, graphene shows minimum conductivity, hence it cannot be turned off completely [79]. The two most successful approaches used for bandgap engineering in graphene are (i) Due to quantum confinement effect in graphene nanoribbons [78], the bandgap could be opened in graphene and (ii) By changing the symmetry in K and K' carbon atoms of honeycomb lattice structure [35]. Therefore, several fundamental material issues need to be addressed before considering graphene for digital electronics.

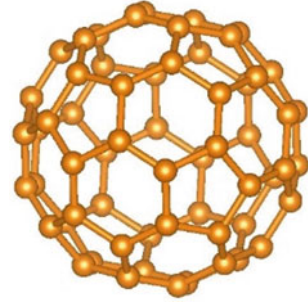
2.4 Graphene for Radio-frequency Transistors

Over the years, owing to superior electronic properties mainly the high mobility of charge carriers, graphene has gained significant attention as a channel material for RF electronics [78]. Lin et al. described a breakthrough study of RF devices fabricated on SiC using graphene, which has 240 nm of gate length [80]. Despite moderate carrier mobility ($1500 \text{ cm}^2/\text{Vs}$), a high operating frequency (f_T) of 100 GHz was achieved. Badmaev et al. developed graphene transistors by a scalable fabrication technique using a T-shaped gate structure (Fig. 7a) [81]. They successfully scaled down the channel length to 110 nm. Guo et al. developed a graphene transistor on silicon-carbon substrate using C-face epitaxial graphene (Fig. 7b) [82]. Significant improvement in the transistor was observed over Si-face epitaxial graphene transistor and a value of 70 Giga-Hertz maximum power gain cut-off frequency was achieved. Self-aligned contacts and high k dielectric T-gate contributed to the maximum frequency value.

3 Carbon Nanomaterials Hybrid-Based Electronic Devices

Hybrids of 0D, 1D, and 2D carbon nanomaterials provide the tremendous potential to obtain next-generation scalable and high-performance devices. Graphene has made significant scientific attention due to its number of uses, such as the conversion of energy and storage, optics, sensors, and electronic devices [83–85]. The electronic device applications of graphene were less due to its gapless nature [86]. Alternatively, chemical changes in various reactive oxygen groups of graphene oxide (GO), enable the development of functional materials used in various applications. Feng et al. [87] fabricated a semi-transparent graphene p–n junction diode, obtained by coating two layers of oppositely charged GO layers, and it has carbon nanotubes electrodes. The current rectification of this diode occurs because the tunneling conduction electrons are governed by an internal field due to this device different from other diodes. The current rectification occurrence in graphene p–n junctions significantly extends the class of materials and physical processes that can be used to design electronic components. This graphene diode can be utilized for simple logic operations such as AND and OR logic gates. Figure 8a shows a high output potential for the AND logic gate if both switches A and B are given positive potential. Unlike the AND gate, OR logic gate has a high output potential, due to either switch A and B, a high potential is triggered as observed in Fig. 8b. Deep et al. [88] reported gate-tunable p–n heterojunction diode by the embedding of n-type single-layer molybdenum disulfide MoS_2 and p-type SWCNTs semiconductors. The heterojunction was formed because these two semiconductors were stacked vertically. The wide range of charge transport is achieved by tuning the heterojunction by the applied gate bias voltage. Under various gate biases, the device's output graphs are shown in Fig. 8c. The p–n

Fig. 1 C₆₀ molecular structure



heterojunction diode often exhibits antiambipolar behavior when handled as a three-terminal device. Figure 8d illustrates junction transfer characteristics, and the green line shows an unusual gate voltage dependence, indicates antiambipolar behavior.

In living systems, metal ion analysis is very important to understand metallic element stabilization and associated diseases [89]. Currently, conventional techniques used for identification and their applications are limited due to time consumption, require sophisticated and costly equipment, and inadequate real-time monitoring. To overcome those limitations, Fan et al. [90] demonstrated the identification of Cu²⁺ ions by functional CQDs modified gate electrodes with the solution-gated graphene transistors (SGGTs). The sensing mechanism of the sensor was channel current varies with the electrical double layer (EDL) capacitance change due to interaction between CQDs and Cu²⁺ ions. Compared to conventional detection methods, the combination of CQDs with SGGTs demonstrates Cu²⁺ detection with a minimum concentration range (1×10^{-14} M). It shows quick response time in seconds. The schematic and working of the SGGT-based Cu²⁺ ion device are shown in Fig. 9 [10].

Over the last few years, research is gaining momentum on new elastic semiconductor materials as they can be integrated into modern, flexible, portable, and handheld consumer electronics [91–93]. So far, carbon nanotubes-based flexible electronics such as flexible and transparent transistors have been fabricated on PET and polymer substrates [94, 95]. Different techniques like floating-catalyst CVD, roll-to-roll transfer, and gas-phase filtration technique employed to fabricate TFT and integrated circuits on flexible transparent substrates [96, 97]. In spite of the significant advances in flexible electronics carbon nanotube and graphene have some obstacles remain. The stretchable transistors need less contact resistance with the channels, electrodes with excellent electrical conductivity and an active channel with a large on–off ratio, both of which point to a cooperation strategy between graphene and CNTs. Electronic device performance-enhanced beyond the flexible electronics by hybrid-based graphene/CNTs [98, 99]. Tung et al. [100] reported solution-based, low-cost scalable, and flexible graphene/CNTs hybrid films show excellent conductivity at high optical transmittance of 86%. This film does not include surfactants to maintain the mechanical and electronic properties of both components. The flexibility of film better than the transparent rigid inorganic crystal structure of ITO suggests maximum compatibility with flexible substrates.

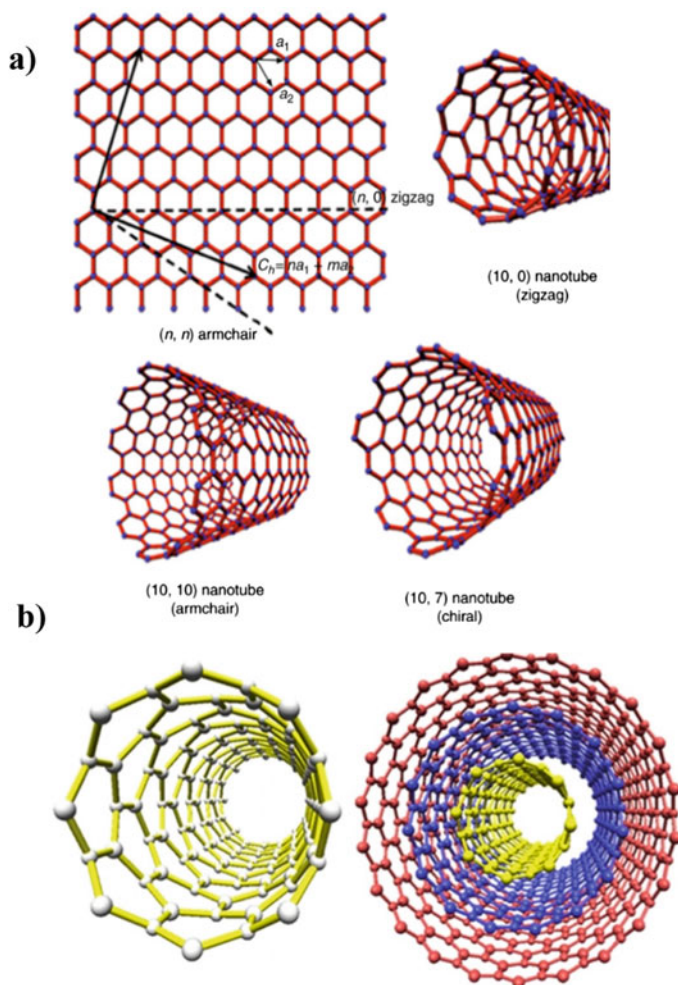


Fig. 2 **a** Schematic representation for different types of CNTs. Reprinted with permission from [25]. Copyright © 2018 Elsevier Inc. All rights reserved **b** Single-walled carbon nanotubes and Multi-walled carbon nanotubes. Reprinted with permission from [26] Copyright @ 202 Springer Nature

4 Carbon Nanomaterials Based Sensors

Based on the types of measurand, sensors are roughly categorized as physical and chemical sensors. Parameters such as strain, temperature, pressure, force, displacement, position, flow rate, etc., mostly are detected using physical sensors. As explained in the introduction, CNTs have excellent mechanical properties with Young's modulus value of 1 TPa approximately for single-walled CNTs [101].

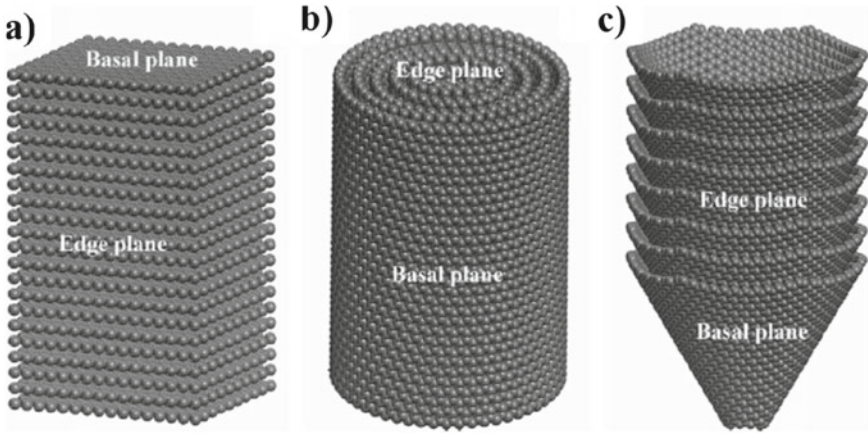


Fig. 3 a–c schematic representation of different carbon nanofiber structures. Reprinted with permission from [29] Copyright © 2012 Elsevier Ltd.

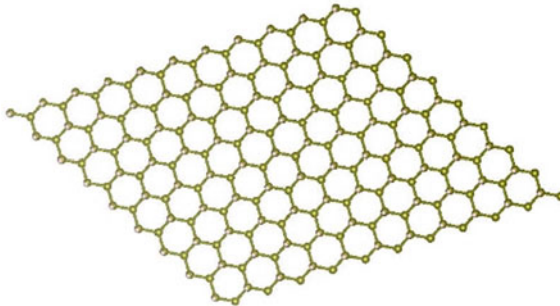


Fig. 4 Schematic illustration of 2D layered graphene structure

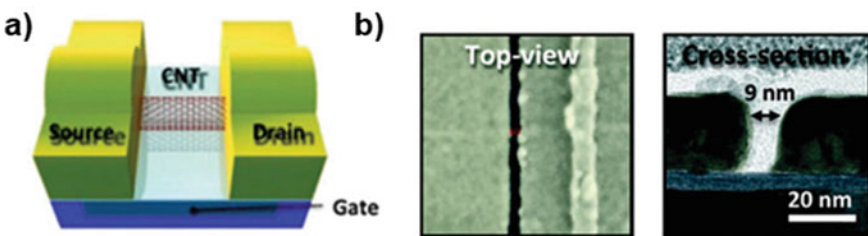


Fig. 5 a CNT FET with bottom gate schematic b Bottom-gate CNT FET with sub-10 nm channel SEM image from top-view and TEM image of the cross-sectional view. Reprinted with permission from [72]. Copyright © 2012, American Chemical Society

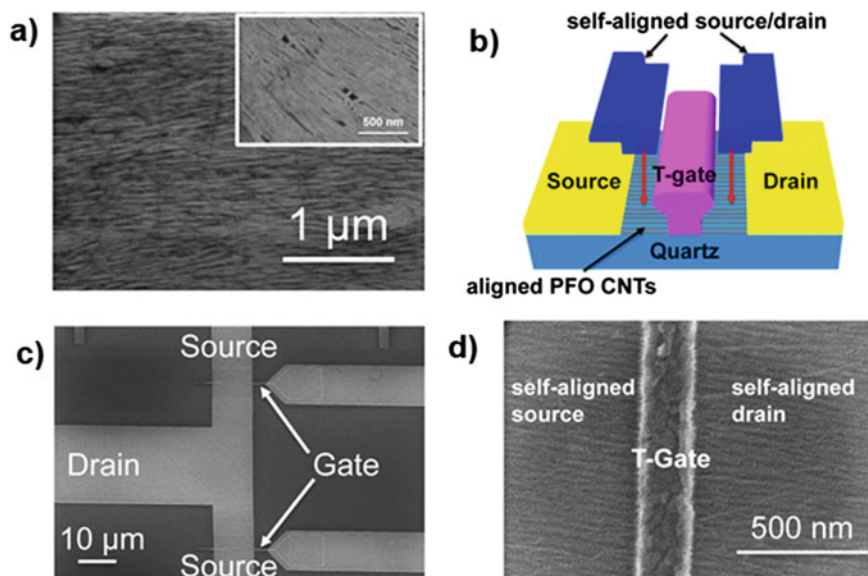


Fig. 6 a SEM graph of Polyfluorene-organized CNT film on a quartz substrate. Approximately 40 nanotubes/μm packing density is seen b Schematic of the self-aligned transistor structure with T-shaped gate c SEM micrograph of the fabricated self-aligned T-shaped gate transistor d High-magnification SEM micrograph of the channel area. Reprinted with permission from [75]. Copyright © 2016, American Chemical Society

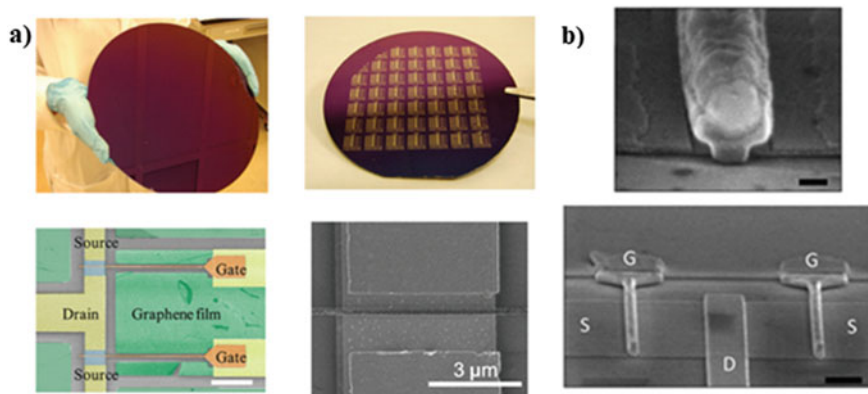


Fig. 7 a 2-inch Silicon wafer with large area graphene (CVD grown). Graphene transistors on Silicon wafer. SEM image (color) of dual-gate graphene transistor (scale bar 10 μm). High-magnification SEM image showing the active area of the transistor. Reprinted with permission from [81]. Copyright © 2012, American Chemical Society b SEM graph (scale bar 100 nm) of the device with 100 nm T-gate with a trilayer resist and drain and source contact metal aligned to the gate foot and a dual-gate graphene FET on C-face SiC (with scale bar 1 μm) Reprinted with permission from [82]. Copyright © 2013, American Chemical Society

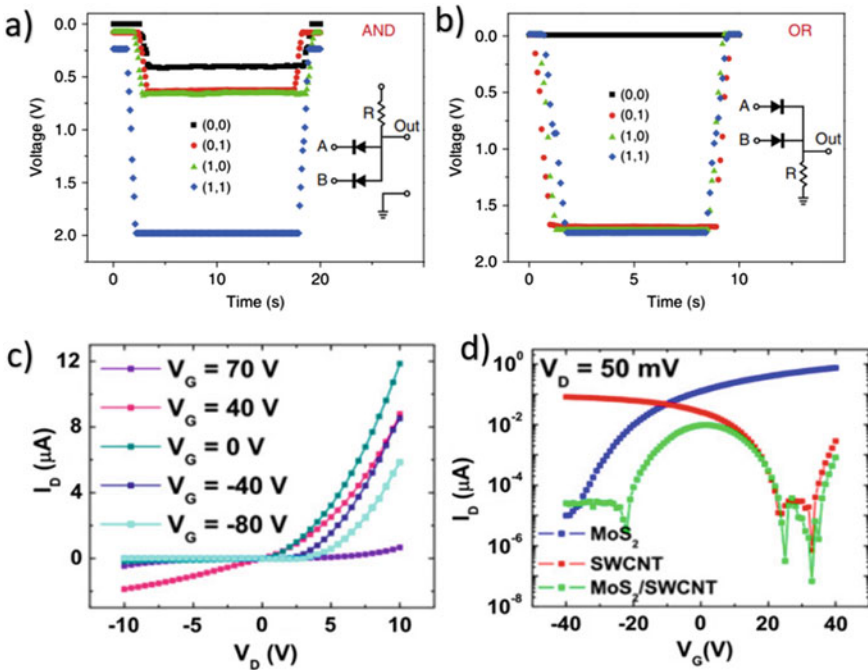


Fig. 8 **a, b** Graphene p-n diode and resistor-based AND and OR logic gates, Reprinted with permission from [87] Copyright © 2018, Springer Nature **c** output characteristics with various gate voltages **d** Transfer characteristics of the p-n junction. Reprinted with permission from [88] Copyright © 2013, National Academy of Sciences

Wong et al. reported an experimental value of 1.28 ± 0.5 TPa for MWCNTs [102]. Also, without any deformation, CNTs showed a high tensile strength (up to 40%).

4.1 Carbon Nanomaterial-Based Pressure Sensor

A pressure sensor is a sensor which converts mechanical displacement into an electrical signal [103–106]. In the last two decades, prominent research has been done in the fabrication of highly sensitive pressures sensor using novel carbon nanomaterials, CNT, and graphene. Zhan et al. reported a wearable and flexible pressure sensor based on SWCNTs/paper through a highly scalable and cost-effective approach with 2.2 kPa^{-1} sensitivity value in a broad range of 35 Pa–2.5 kPa and 1.3 kPa^{-1} sensitivity in 2500–11,700 Pa [107]. The sensor was fabricated by impregnating SWCNTs into paper and sandwiched between a PDMS film and PI sheet that is decorated with interdigitated gold (Au) electrodes (Fig. 10).

Sahatiya et al. demonstrated a flexible, biodegradable pressure sensor by sandwiching MWCNTs between PI substrate and cellulose paper. Multi-walled CNTs

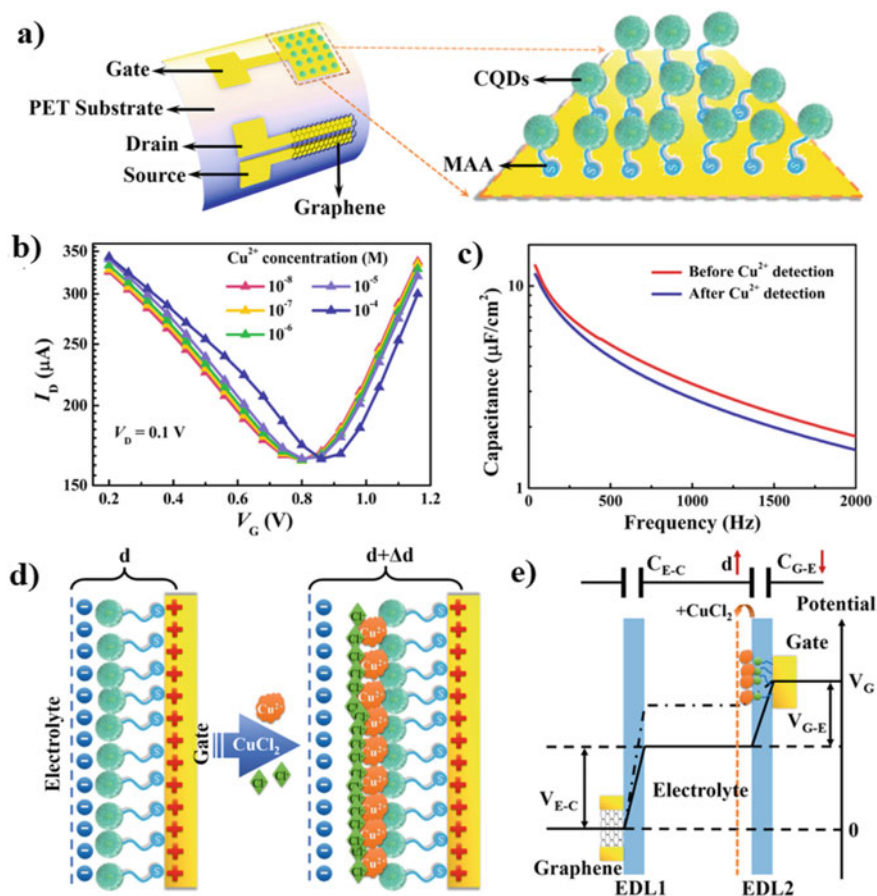


Fig. 9 a SGGT-based Cu^{2+} ion sensor b Transfer curves of SGGT c frequency and gate capacitance relationship before and after Cu^{2+} ions are added d Schematic illustration of the EDL capacitance variation mechanism e Potential drops on the surface of graphene channel and gate, across the two EDLs. Reprinted with permission from [90]. Copyright © 2020, American Chemical Society

were deposited on the substrate (PI) by roll pin and pre-compaction mechanical pressing technique (Fig. 11a) [108]. Sensitivity value of 0.549 kPa^{-1} was seen by a fabricated pressure sensor and a response time of lesser than 32 ms. Furthermore, the fabricated pressure sensor was used as a touchpad and electronic skin application. Graphene was widely used as active as well as inactive material for pressure sensor applications. Although graphene no piezoelectric properties, it was used as electrodes to support piezoelectric material and also used as an additive to piezoelectric polymer like PVDF to improve piezoelectricity [109]. Furthermore, due to graphene's excellent mechanical and electronic properties, it has been extensively used as an active material for the piezoresistive pressure sensor as elucidated in the introduction. Zhu et al. developed a piezoresistive pressure sensor using graphene

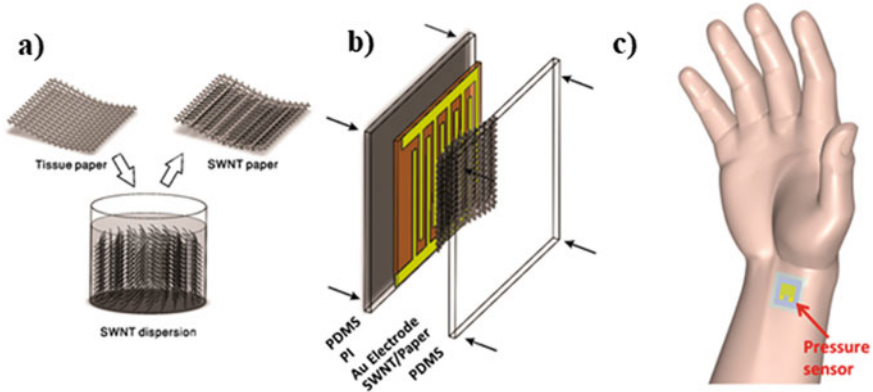


Fig. 10 Pressure sensors fabrication process illustration. **a** The SWNTs were dip-coated on tissue paper **b** Single-wall nanotube/tissue paper is accumulated onto gold electrodes on a PI substrate; encapsulated using PDMS layers which provides mechanical support and **c** To sense heart pulse human wrist is mounted with a pressure sensor Reprinted with permission from [107]. Copyright © 2017, American Chemical Society

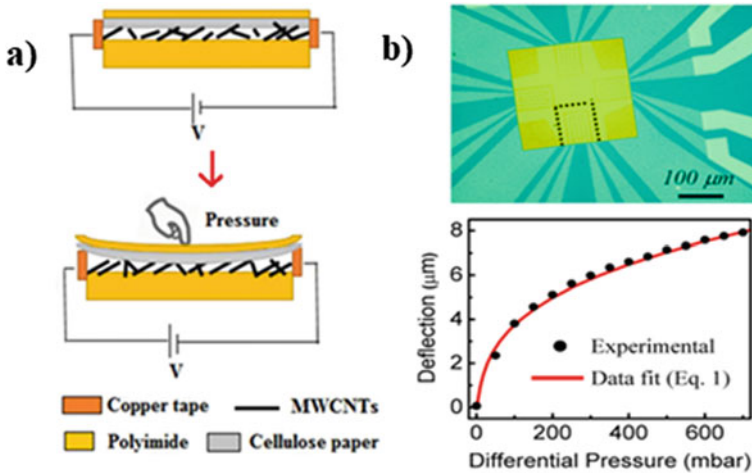


Fig. 11 **a** Ultrasensitive touchpad schematic which is done by sandwiching MWCNTs between polyimide and cellulose paper [108] **b** Silicon nitride square membrane with graphene piezoresistors optical microscope image (the dotted lines indicate the device used) and SiN membrane with deflection v/s differential pressure of 100 nm. Reprinted with permission from [110] Copyright © 2013, American Institute of Physics

on the silicon nitride membrane showed a dynamic range of 0–700 mbar [110]. In this strain sensor, multilayer polycrystalline was fabricated using a chemical vapor deposition method (Fig. 11b). Yao et al. developed a pressure sensor using a flexible graphene/polyurethane sponge using a fracture microstructure [111]. PU

sponge which is available commercially was coated with graphene oxide using the dip-coating technique and then it was reduced to improve thermal conductivity using hydrogen iodide, further softened with hydrothermal treatment. The fabricated sensor exhibited a sensitivity of 0.26 kPa^{-1} (0–2 kPa range) and 0.03 kPa^{-1} (2–10 kPa). The fractured microstructure improved the sensitivity when compare with rGO/PU sponge sensor without fractured microstructure. Jian et al. fabricated a graphene/CNT hybrid-based highly sensitive pressure sensor [112]. Because of the synergistic effect in the hybrid, the fabricated pressure sensor exhibited a high sensitivity of 19.8 kPa^{-1} and a very small detection limit around 0.6 Pa. Tian et al. reported a pressure sensor that is sensitive to a 0–50 kPa wide pressure range using laser scribe graphene with a foam-like structure. The sensitivity value of 0.9 kPa^{-1} was seen using this pressure sensor [113].

4.2 Carbon Nanomaterials-Based Strain Sensor

Lee et al. presented a fully microfabricated strain sensor by SWCNT film on PI film. Polyimide was prepared by spin coating glass wafer and photolithography was used for patterning the electrode [114]. Later, by using a spray coating method, 280-nm-thick CNT film was deposited on PI film. The fabricated device showed a linear relationship between the applied strain and resistance over a range from 0 to 400 microstrain and a high gauge factor of 60. Dharap et al. demonstrated a strain sensor using pristine-SWCNTs film using vacuum filtration by 0.2 mm Teflon membrane [115]. The SWCNTs thin film was attached to a brass specimen and the results showed that the relation between the applied strain and change in the voltage across the film is linear. In the last few years, MWCNTs have attracted the researchers' interest due to relatively higher purity, cost-effectiveness, and superior electronic properties in comparison with SWCNTs. Zhang and co-workers have fabricated strain sensors based on silver nanoparticles and MWCNTs on flexible PDMS substrates (Fig. 12) [116]. The sensor exhibited gauge factors that are tunable in the range of 2.1–39.8 and stretchability of 95.6%. Further, the sensitivity and linearity of the sensor could be adjusted by Ag NPs concentration.

Zhao and co-authors demonstrated the very sensitive strain sensor using nanographene films on the mica substrate [117]. Fabricated sensor achieved a gauge factor of more than 300. Li et al. demonstrated a strain sensor using graphene woven fabrics (GWFs) on the PDMS substrate [118]. SWFs were prepared using a woven copper mesh by a CVD process and later copper was etched away. After placing GWFs on PDMS, contacts were taken using silver paste (Fig. 13). The fabricated sensor achieved an approximate value of 10^3 gauge factors for 2–6% strains and $\sim 10^6$ for greater than 7% strains. The ultrahigh sensitivity of the device was ascribed to mesh configuration and fracture behavior of graphene micro ribbons.



Fig. 12 CNTs/PDMS strain sensor fabrication process which is modified using silver nanoparticles. The as-prepared product is illustrated in the center. Reprinted with permission from [116]. Copyright © 2015, Elsevier

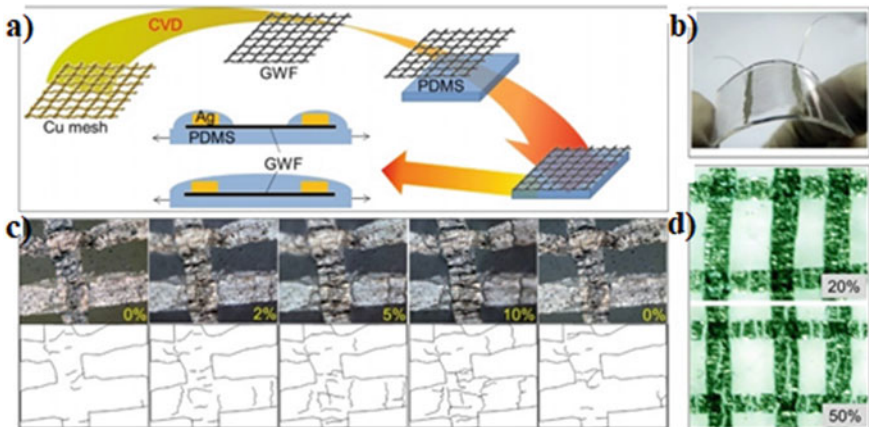


Fig. 13 a Schematic illustration of GWF/PDMS fabrication b Wired samples macroscopic optical image c Establishment of crack and their evolution in GWF with various strain optical images, and schematic illustration d large strains GWF Optical images (20 and 50%) Reprinted with permission from [118]. Copyright © 2012, Springer Nature

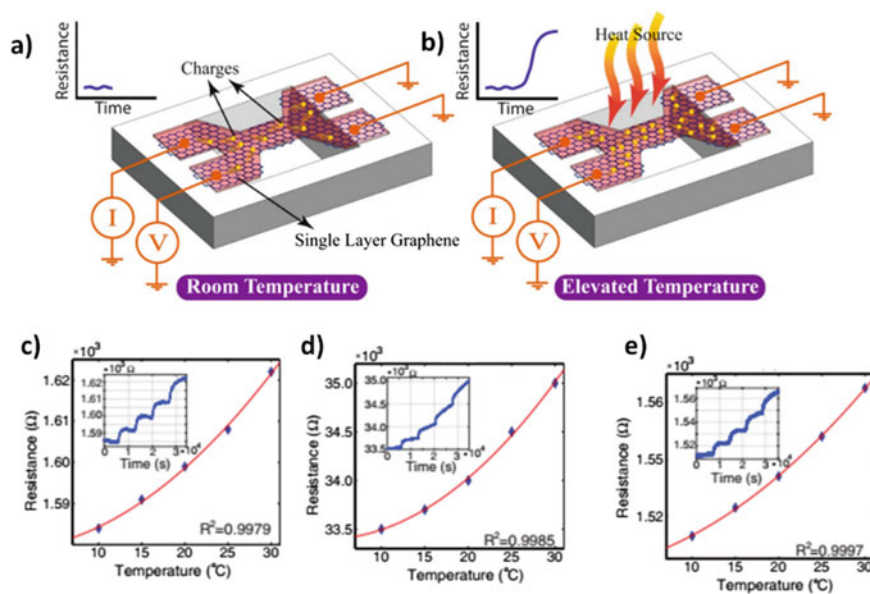


Fig. 14 a Graphene sensors schematic illustration. With the temperature rises from room temperature to a high temperature b, Mobility will be decreased due to a proportionate increase in the number of electrons. A resistance varies in terms of temperature and time for the three different graphene sensors: c on a SiO_2/Si substrate, d on a SiN membrane e the deferred graphene sensor. Reprinted with permission from [119]. Copyright © 2017, Springer Nature

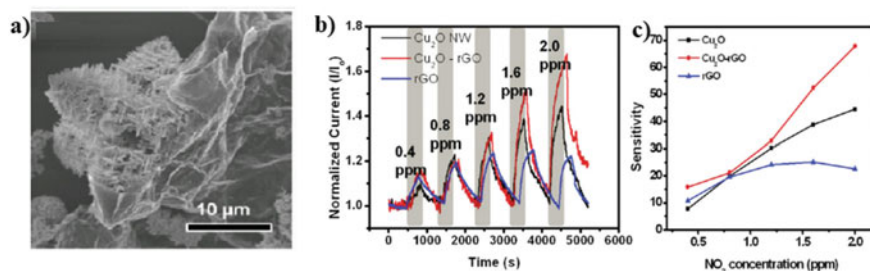


Fig. 15 a Scanning electron microscope image of rGO/ Cu_2O nanowire mesocrystal, b Dynamic response of different hybrid carbon nanomaterials under the exposure of NO_2 gas with increased ppm levels, c sensitivity of three devices (Cu_2O , Cu_2O -rGO, and rGO) are plotted. Reprinted with permission from [145]. Copyright © 2012, American Chemical Society

4.3 Carbon Nanomaterials-Based Temperature Sensor

Temperature sensor is a crucial part in several major applications, such as health monitoring, artificial electronic skin, etc. Resistive-based temperature detectors are the most widely used sensor due to their high accuracy, stability, fast response.

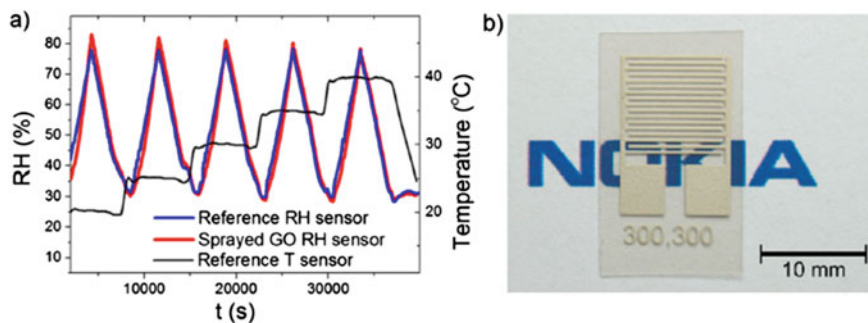


Fig. 16 a Sensing performance of GO RH sensor of 15 nm thick compared with commercially fabricated RH sensor with high-performance b Image of GO film sprayed on Ag electrodes. Reprinted with permission from [158]. Copyright © 2013, American Chemical Society

Furthermore, thermal sensors, mercury thermometers, and infrared temperature sensors are also widespread. In the past few years, carbon-based sensitive materials including graphene, CNTs, and carbon fiber have gained more attention for temperature sensor applications due to their extraordinary mechanical and electronic properties compared to ceramics, metals, metal oxides. Davaji et al. developed a temperature sensor based on single-layer graphene on three dissimilar substrates, a silicon nitride membrane, a silicon/silicon dioxide-based substrate, and a suspended architecture (Fig. 14) [119]. The fabricated temperature sensors acted as a resistive type, and the resistance change was explained using electron–phonon scattering and electron mobility–temperature relationship ($\sim T^{-4}$). From the analysis, the team revealed that the silicon nitride membrane-based sensor shown the highest sensitivity because of a smaller value thermal mass and it has shown the lower value of sensitivity for the sensor on SiO_2/Si . Furthermore, the sensor on silicon nitride showed improved mechanical stability in comparison to the deferred graphene sensor. Sahatiya et al. demonstrated flexible wearable temperature sensors based on flakes of graphene and solar exfoliated reduced graphene oxide (SrGO) on the PI substrate [120]. Both graphene flakes and SrGO based temperature sensors discovered a negative temperature coefficient that was comparable with commercial temperature sensors. This research has clearly shown that graphene on a flexible PI substrate could be used effectively as wearable temperature sensing applications.

4.4 Carbon-Based Nanomaterials for Chemical Sensors

A device that converts the existence of target compounds into a computable quantity is called a chemical sensor [121]. Gas sensors, vapor sensors, humidity sensors, etc., used for the detection of target compounds are different types of chemical sensors [122–126]. A detailed explanation of carbon-based nanomaterials used to detect target compounds is depicted below.

4.4.1 Carbon-Based Nanomaterials for Gas Sensors

The measurement and existence of concentration of a specific gas in the earth's surrounding atmosphere such as natural fumes, dangerous gases, etc., are detected by using a device known as gas sensor [127]. These sensors are used for monitoring the environment [128], control of hazardous gas emissions, production control in cultivation and health diagnostics, etc. [129–131]. Over the years, researchers have utilized carbon nanomaterials like graphene, GO, rGO, CNTs, etc., and found them as efficient candidates for gas sensing applications. Chemiresistors, field-effect transistors, Schottky diode, etc., are different configurations of device architecture for gas sensing [127]. Novoselov and his co-workers utilized graphene for the first time for fabricating gas sensors in 2007 to detect NO₂ gas [132] graphene-based sensing devices are fabricated using graphite flakes which are exfoliated micro-mechanically and supported on Si substrate. These fabricated devices have shown remarkable sensitivity for detecting individual gas molecules. Later in 2009, Dan and his co-workers proved that the pristine graphene-based device fabricated by Nove Selo has improved its sensitivity by forming a contamination layer on the graphene on Si substrate using an electron-beam lithography technique [133]. This layer helps to detect various other individual molecules such as octanoic acid, H₂O, nonanal, and various other gas vapors which are down to ppm level. Balandin and his co-workers also employed an electron beam lithography technique for fabricating the FET device using pristine graphene and with the help of low-frequency noise of the device they detected various organic vapors [134].

Later, CVD technique was used for fabricating a sensing device using graphene sheets in the layered form with exceptional quality on Si substrate to detect gases such as ammonia [135, 136], carbon dioxide, nitrous oxide [137, 138], and also used to detect humidity [139]. Gautam et al. deposited graphene monolayers on the Si support to detect CH₄, H₂, and NH₃ [135]. Improved sensitivity is observed using this device by operating it at a temperature range between 150 and 200 °C but there is no enhancement in response time [135]. Choi et al. fabricated a sensing device where SLG (single-layer graphene) is used as an active component and BLG (bi-layer graphene) is used as a heating element that can heat up to 200 °C [140]. This device achieved a response in the range of 39% to 41 ppm of NO₂ and further, the existence of the element for heating facilitated to upsurge the retrieval time of the device. In the future, a lot of modifications (such as the incorporation of defects and impurities) should be done to pristine graphene to improve its selectivity, sensitivity, and durability of the fabricated sensing device. Graphene oxide is also used for sensing various gases owing to the presence of oxygen-containing functional groups in its structure. To improve the sensing activity of the graphene oxide device it is further reduced in an atmosphere such as hydrogen (Via thermal route) to obtain rGO. In 2008, Robinson and his co-workers first used rGO based devices for detecting various gases [141]. Initially using the spin coating method GO is deposited on the Si substrate and later reduced with reducing agent vapors of hydrazine to fabricate rGO-based sensing device at 100 °C. Manohar et al. fabricated rGO-based flexible printed sensing device which is prepared using an ascorbic acid reducing agent [142]. This

Table 2 Different carbon-based nanomaterials gas sensing performance for detecting various gases

Material	Detected gases	Response/ Retrieval time	Detection limit	Sensitivity (response x ppm^{-1})	Reference
Single Layer graphene / Bilayer graphene (CVD)	Nitrous oxide	95 s/11 s	–	0.98%	[140]
Single Layer graphene (CVD) patterned	Nitrous oxide, Ammonia	89 s/579 s	–	2.6% (Nitrous oxide)	[139]
PANI/reduced graphene oxide	Hydrogen	2 min/3 min	–	0.0016%	[146]
CNTs/graphene oxide	Nitrous oxide	1 h/3 h	0.5 ppm	2%	[147]
In_2O_3 / reduced graphene oxide	Nitrous oxide	3 min/4 min	–	12.2%	[148]
ZnO Ncryst/ reduced graphene oxide	Methane	1 min/10 s	100 ppm	0.05%	[149]

device was fabricated using the inkjet printing technique by dissolving rGO in water in the existence of surfactant and displayed a positive response with increased resistance behavior in detecting dichloromethane and various alcohols, negative response detection behavior to Cl_2 and NO_2 . Furthermore, different carbon nanomaterials-based hybrid composites are employed to enhance the sensitivity and selectivity of these gas sensors. Chung et al. fabricated a flexible device using CVD graphene which is decked with palladium nanoparticles to further improve the sensitivity to 30 for 1% of H_2 gas detection [143]. Wu et al. used a nanocomposite thin-film device which was prepared using graphene extracted using exfoliation and PANI for detecting methane gas in ambient temperature conditions [144]. This device has shown a considerable amount of 10% response to 10 ppm of gas. Using hydrothermal method Deng et al. synthesized rGO/ Cu_2O nanowire mesocrystals which are integrated to detect NO_2 gas [145] (Fig. 15). Furthermore, there is a lot of scope for various hybrid carbon-based nanomaterials that are used for detecting various gases by fabricating suitable gas sensors. The sensing performance of the various carbon-based gas sensors is tabulated in Table 2.

4.4.2 Carbon-Based Nanomaterials for Humidity Sensors

The water vapor existing in the air is known as humidity which is measured as relative humidity (RH). The relative humidity is defined as the fraction between the fractional

pressure of water and the vapor pressure at equilibrium at a given temperature. These sensors are mostly used in agricultural sectors and industries for keeping a track of the quality of food in food processing industries, medical equipment, weather prediction, etc. Polymers [150], metal oxides [151, 152], porous silicon [153, 154] are mostly used for commercial humidity sensors. Exceptional qualities such as larger sensing areas and high chemical inertness made researchers use carbon nanomaterials for humidity sensing applications. Zhang et al. synthesized carbon nanosheets and honeycombs in the nano range on Si substrates using a hot filament PVD (physical vapor deposition) technique and observed that carbon nanosheets have shown remarkable sensing response 11–95% humidity range under ambient conditions [155]. Luo et al. manufactured and characterized quartz crystal microbalance (QCM) humidity sensor using a sensitive layer made by graphene oxide [156]. This QCM humidity sensor has shown a 10–60% sensing range, 1371(Q)/1% relative humidity, a recovery time of 3 s, and a response time of 20 s. Yadav et al. synthesized multiwalled CNTs using the direct liquid injection CVD method on cobalt substrate and utilized for designing humidity sensors to sense moisture with RH in the range of 10–90% for various applications [157]. Very recently, Borini et al. fabricated graphene oxide (GO) based humidity sensors using a spray coating method on silver electrodes (GO thin-films typically in the range of ~15 nm) [158]. Figure 16a depicts that GO-based thin film has shown characteristics almost similar to that of commercially available RH sensors. In Fig. 16b, GO-based thin film is almost invisible (i.e., it is in the order of few nm).

5 Carbon Nanomaterials-Based Electrochemical Sensors

Various nanomaterials such as carbon-based [8, 159], transition metal dichalcogenides [160], noble metals [161, 162], etc., are used for electrochemical detection. Among them, nanomaterials based on carbon are extensively used for electrochemical (electroanalytical and electrocatalytic) sensing due to their improved capability to transfer electrons in electrochemical reactions. Mostly reported carbon nanomaterials for electrochemical sensing are graphene [163, 164], CNTs [165, 166] fullerenes [167], carbon nanofibers [168], and carbon quantum dots [169], etc. These all nanomaterials when utilized for electrochemical sensing are either used in their pristine form/mixed with new materials/functionalizing their pristine form during device fabrication. Electrochemical sensing of the above-mentioned carbon-based nanomaterials is reviewed below.

5.1 CNTs-Based Nanomaterials

In the study of electrochemistry of carbon nanomaterials, electron transfer is surface-dependent. Electron transfer is improved by adding functional groups on the surface

of these materials. Britto et al. first applied carbon nanotubes in electrochemistry as electrodes [170]. They concluded that the immobilization of activated CNTs on the surface of the electrode is the major drawback for electrochemical sensing applications because of their insolubility property in almost all solvents which would result in nonuniform and unstable films. To avoid this problem, different physical/chemical methods are used for dissolving CNTs first in various solutions and immobilizing on different electrode surfaces. Immobilization of CNTs on electrode surfaces is done using various methods that are used for electrochemical sensing applications which are explained in detail below.

- (i) **Solvent dispersion and immobilization by casting:** In this method, initially CNTs are cleaned/purified and activated by pretreatments then dispersed in solvents such as DMF [171, 172], toluene [173, 174], etc., using ultrasonication process and later this mixture is dropped on to the surface of electrode followed by drying it (i.e., casting) for electrochemical detection of analytes.
- (ii) **Additive assisted and immobilization:** In this method, additives such as surfactants, polymers are added into the solvents where CNTs are dispersed to enhance the stability and solubility of the solution (i.e., solution doesn't get settled easily) and then subjected to immobilization for applying in electrochemical sensing applications.
- (iii) **Carbon nanotube paste electrodes:** In this method, paste electrodes are fabricated using binders in liquid form and CNTs. These paste electrodes made from CNTs hold the properties of the old-style carbon paste electrodes (CPEs), for example, the attainability to consolidate different substances, the low currents in the background, the wide range of potential, and the composite nature. These electrodes also reserve exceptional electrochemical properties that enhance the electron transfer mechanism which is useful for increasing the efficiency for electrochemical detection of various analytes especially biomolecules. The carbon paste electrode fabrication doesn't require any pretreatment for CNTs (SWCNTs and MWCNTs) which are used.

Properties such as easily modifiable surface, solid electrocatalytic activity, the tube-like structure of CNTs in nano range (which helps to increase the surface activity), etc., have made CNTs unique materials for electrochemical sensing applications.

5.2 Graphene-Based Nanomaterials

Graphene is a two-dimensional material that has a single layer of sp^2 hybridized carbon atoms extracted from three-dimensional graphite and closely packed into a hexagonal lattice structure.

5.2.1 Graphene Oxides-Based Electrodes

Initially, GO aqueous electrolyte solution was prepared by using conventional methods of chemistry such as modified hummers methods which are used in the preparation of electrode materials using two-dimensional graphene for electrochemical sensing applications. In the next step, as prepared GO solution is dropped onto the surface of electrodes such as glassy carbon electrode [175, 176], gold electrode [177], disk shape platinum electrode [178]. For activating the carboxylic acid groups present in GO, the GO-coated electrode is immersed in buffer solutions such as EDC, NHS which helps in the formation of a covalent bond between electrode and enzyme [178]. This prepared electrode is used for the recognition of various target analytes based on its electrochemistry. The above mentioned prepared graphene-based sensors are used as enzyme biosensors, non-enzymatic biosensors that are applicable for simple biomolecules, immunosensors, etc. The performance of various graphene-based electrodes for electrochemical sensing is tabulated in Table 3.

6 Carbon Nanomaterials-Based Resistive Memories

Technology based on semiconductor devices has been improving rapidly by a decrease in their size. Advanced semiconductor device fabrication uses nanotechnology, where critical dimensions of these devices are found to be around 20 nm. These devices are categorized into display devices, memory devices, logic devices, etc. Among them, memory devices with large density, high-performance, and lower consumption of power are in great demand [183]. Portable electronic devices have unique non-volatility (where memory is not lost even when the device is off). These non-volatile memory property-based devices are further classified into flash memory and resistive switching memory devices [184]. A three-dimensional structure consisting of an insulating layer between two electrodes with a simple configuration is the resistive switching memory cell in the ReRAM device. Resistive exchanging memory gadgets use the contrast in opposition to the high and low resistance memory states and have a straightforward gadget structure (metal/separator/MIM metal structure) relevant to high-thickness memory gadgets with a minimal creation cost [184–187].

From Fig. 17 it is clear that the resistance of a resistive memory device is switched from high to low state and vice versa by applying an appropriate voltage to the device [188–190]. Recently, researchers around the world widely studied and found that nanomaterials like metal chalcogenides, metal oxides, carbon-based materials are suitable candidates for resistive-based memory devices [188–192]. Among them, carbon-based nanomaterials are found as efficient for non-volatile resistive-based memory devices [193].

Table 3 Carbon-based nanomaterials performance for electrochemical glucose sensing

Graphene-based materials	Linear range (mM)	Detection limit (μM)	Sensitivity ($\mu\text{AmM}^{-1}\text{cm}^{-2}$)	Reproducibility: RSD for (No. of electrodes)	Stability, % of initial response after (days)	References
CrGO	0.1–10	10 ± 2	110 ± 3	2.5% (6)	No obvious decrease (2 days)	[179]
CrGO-AuNPs	0.1–10	35	–	0.74% (3)	80% (4 months)	[180]
Sulfonated rGo-CdS	2–16	700	1.76	4.2% (5)	93% (30 days)	[181]
CrGO-Ni (II)-quercetin	0.003–0.9	0.5	187	5.1% (7)	92.1% (20 days)	[182]

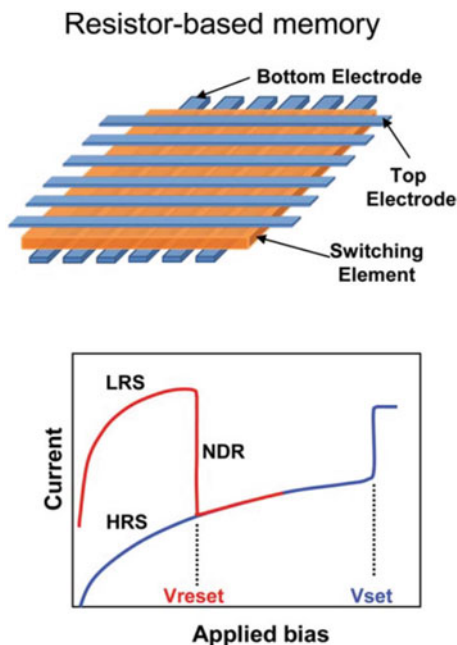


Fig. 17 Schematic of the resistive-based memory device and its operation (low resistance state, high resistance state, and negative differential resistance are LRS, HRS, and NDR, respectively). Reprinted with permission from [183]. Copyright © 2011, Royal Society of Chemistry

Graphene-based nanomaterials such as GO, rGO, hybrid GO, and hybrid rGO are used as dielectric materials in nonvolatile resistive-based memory devices which are depicted in Fig. 18. Rani et al. experimentally found that graphene-based non-volatile memory devices (pristine and hybrid GO, rGO materials) are having a broad range of scope for the advancement of new flexible memory applications by evaluating device characteristics [191]. Tsai et al. have demonstrated that CNT/ AlO_x /CNT material-based crossbar electrodes for RRAM device with current programmed around 1 nano ampere and ON/OFF ratio up to 5×10^5 have capable characteristics for non-volatile memory devices [194]. By embedding a graphene single-layer sheet into the interface between a transparent top cathode (formed of Indium-doped tin oxide substrate) and a zinc oxide resistive-exchanging layer, transparent RRAM innovation can be upgraded [195]. The resulting resistive RRAM (random access memory) device displays better-exchanging conduct with elevated exchanging yield and consistency than those of the gadget absence of graphene.

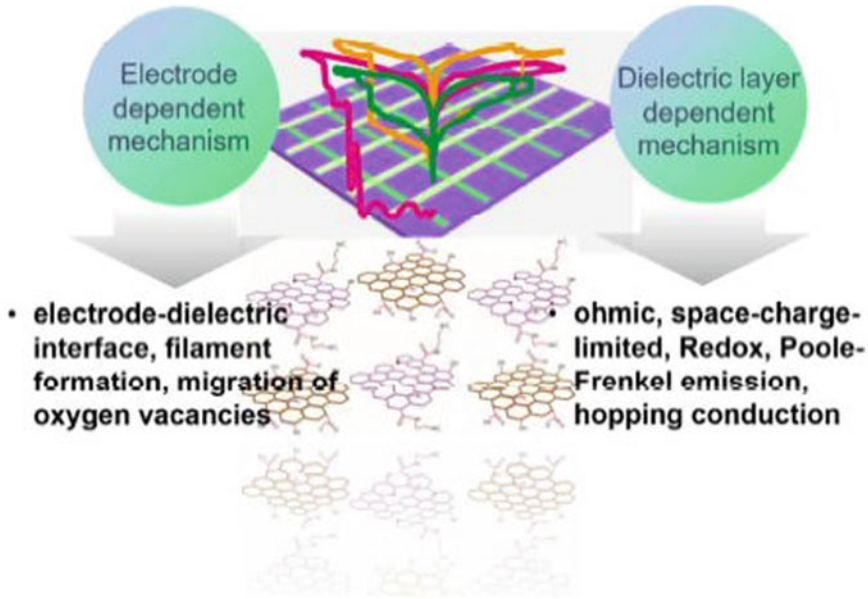


Fig.18 Mechanism of ReRAM device using graphene-based materials. Reprinted with permission from [191]. Copyright © 2016, Royal Society of Chemistry

7 Carbon Nanomaterials-Based Photodetectors

The photodetector is a semiconductor device that converts illuminated light into a precise electrical signal, photovoltage, or photocurrent [51, 196–199]. Photodetectors are considered as an interface among electrical circuitries and optical information. Therefore, photodetectors have several applications in digital imaging, security, environmental monitoring, digital communication [200]. Carbon nanomaterials have excellent optoelectronic properties with the potential of substituting inorganic semiconductors and metals. GQD, carbon allotropes (CQD), buckyballs, CNTs, graphene-based materials are extensively used in the fabrication of photodetectors because of their larger values of absorption coefficients and carrier mobility, tunable bandgap [201–206].

7.1 Fullerene Based Photodetectors

Fullerenes show a strong absorption below 400 nm, which could be utilized for UV light detection. Ma et al. showed Buckminster fullerene (C_{60}) electronic potential in electronic devices, by forming a C_{60} -diode of relatively modest architecture [207]. C_{60} was inserted in between aluminum (anode) contact and an ohmic

copper (cathode), forming a diode that can withstand a very high current density of 363 A/cm^2 . Szendrei et al. demonstrated hybrid thin-film photodetectors based on fullerene and PbS nanocrystals with a spectral range of visible and NIR regions up to 1300 nm [208]. The maximum responsivity at 514 nm is 1.6 A/W value which is recorded. Furthermore, sturdy gate dependence and electron mobility values up to $3 \times 10^{-4} \text{ cm}^2/\text{Vs}$ are displayed by the device. Guo et al. demonstrated fullerene-based organic photodetector (OPD) on ITO glass with very little noise current and at 3470 nm , a high detectivity of $3.6 \times 10^{11} \text{ Jones}$, 90 dB of broad linear dynamic range (LDR), and a response speed greater than 20 kHz [209].

7.2 Graphene Quantum Dots Photodetectors

In GQD, the optical bandgap is strongly influenced by quantum confinement and edge effects. In GQD, bandgap tuning has been investigated and is considered to be an important advantage in optoelectronics over plane graphene and bandgap decreases with an increase in quantum size. A key absorption in the ultraviolet region is shown by graphene-based quantum dots. Zhang et al. fabricated a superior performance deep UV photodetector using GQD. Using a facile hydrothermal method, GQDs were synthesized with an average particle diameter of 4.5 nm and displayed a bandgap of 3.8 eV due to the quantum confinement effect which leads to an absorption peak found around the wavelength of 320 nm (Fig. 19) [210]. The built-in electric field was created due to the difference between work function of GQDs and two metal electrodes which is the major reason for extraction efficient photocurrent. The responsivity and detectivity of the photodetector were 2.1 A/W , $9.59 \times 10^{11} \text{ Jones}$, respectively. Tang et al. synthesized n-doped GQDs using a microwave-assisted synthesis method. N-doped GQDs shown a wide absorption range covering UV, vis, and NIR range (300 to $>1000 \text{ nm}$) [211]. The UV absorption was ascribed to the transitions in $\text{C}=\text{N}$, $\text{C}=\text{O}$, and $\text{C}=\text{C}$ bonds. The visible absorption is caused by extended partial conjugated π -electrons in single layers of paper. Absorption in the NIR region is due to the absorption is ascribed to the delocalization of π -electrons due to the layered structure. The responsivity at various excitation wavelengths was calculated to be at 365 nm , 405 nm , 808 nm , 980 nm wavelengths are 1.14 V/W , 325 V/W , 10.91 V/W , 10.91 V/W , respectively.

7.3 CNTs-Based Photodetectors

CNTs display opportunities for novel photodetectors because of their remarkable optical properties. Free electron–hole pair excitations and also strongly bound electron–hole pair states are called excitons present in semiconducting CNTs which have a direct bandgap. The exciton binding energy of carbon nanotubes depends on the diameter and dielectric constant of the surrounding environment. In recent years,

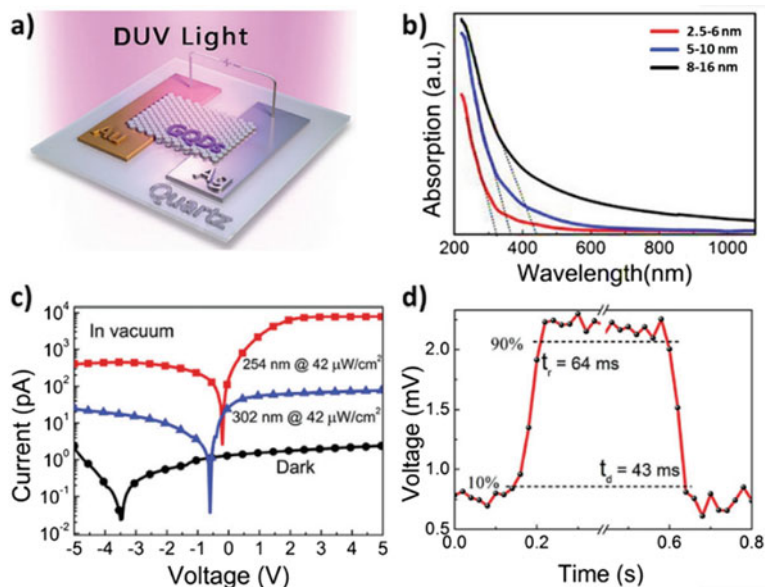


Fig. 19 a) GQDs used photodiode structures illustration b) Using particle size, the absorption performance of GQDs can be tailored c) Current–voltage characteristics of the Au/GQDs/Ag diode. The photocurrent and rectification behavior is increased by a decrease in wavelength d) The photovoltage had a response time and fall time of 64 ms, in response to a light pulse at the wavelength of 254 nm (43 ms) Reprinted with permission from [210]. Copyright © 2015, American Chemical Society

several research groups have reported that photocurrent could be produced in a CNT when illuminated, which is in contact with metal electrodes. The charges are separated due to the Schottky barrier on the metal–CNT interface that provides an internal electrical field. Rao et al. studied the photoconductivity of the pure CNT film. They developed SWCNTs on SiO₂/Si substrates using CVD across a channel in the layer of SiO₂ and 8–20 CNTs have connected the channel [212]. Alternative methods for charge separation are establishing p–n junction, applying asymmetrical metal contacts. Liu and co-authors demonstrated a photodiode using purified SWCNTs deposited on n-Si/SiO₂ by liquid phase, wherein asymmetrical metal contacts were used [213]. The I–V characteristics were well matched with the conventional diode equation which was ascribed to reduced defects in SWCNTs. Peak responsivity attained was $1.5 \times 10^8 \text{ V W}^{-1}$ and above 107 V W^{-1} for the wavelengths ranging between 1200 and 2100 nm. In a similar spectral range, detectivity stayed above 10^{10} Jones and achieved a peak with 1.25×10^{11} Jones at 1800 nm.

He et al. developed a photodetector by developing highly aligned SWCNTs between two Au contacts, where to establish p–n junction, half the intrinsically P-type CNTs were n-doped (Fig. 20) [214]. The highly aligned SWCNTs provide an extended absorption spectrum range from 3 μm to 3 μm . The responsivity was

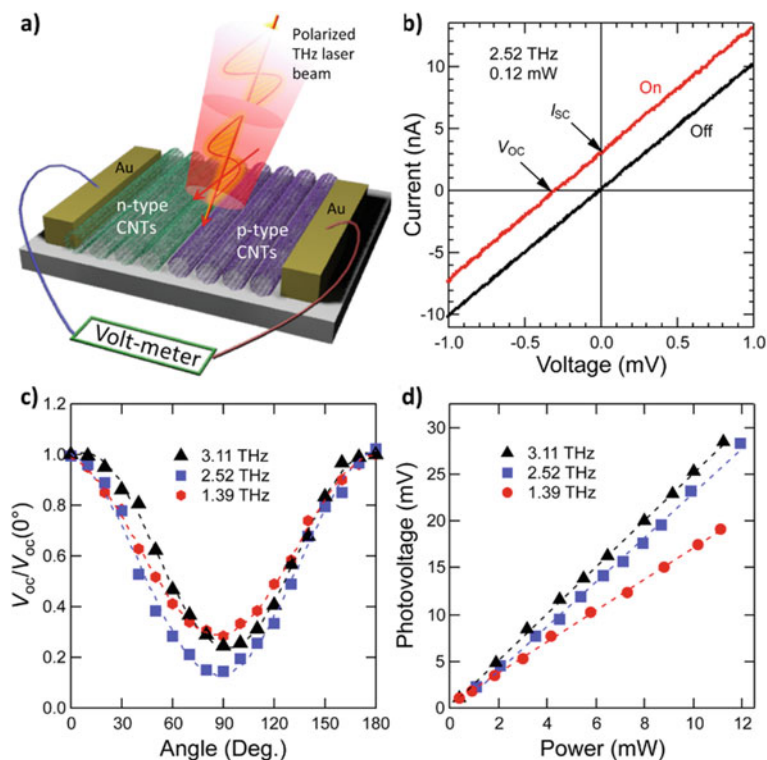


Fig. 20 Carbon nanotube Terra-Hertz detector characteristics. **a** Experimental geometry-based diagram schematic illustration. Linearly polarized Terra-Hertz beam is illuminated on the device at room temperature and I–V characteristics are measured **b** Graph showing the I–V characteristics without illumination and with the illumination of 2. THz beam **c** Polarization dependence of open-circuit voltage (V_{OC}) for frequencies of 3.11 THz, 2.52 THz, and 1.39 THz which was normalized by its value for parallel polarization, **d** Power dependence of V_{OC} for frequencies of 3.11 THz, 2.52 THz, and 1.39 THz, showing responsivities of 1.7 V/W, 2.4 V/W, and 2.5 V/W, respectively. Reprinted with permission from [214]. Copyright © 2014, American Chemical Society

observed to be 2.5 V/W at 96.5 μm (3.11 Tera-Hertz), 2.4 V/W at 19 μm (2.52 Tera-Hertz), and 1.7 V/W at 215 μm (1.39 Tera-Hertz). Liu et al. demonstrated hybrid broadband photodetector (across visible to NIR range, 400–1550 nm) using atomically thin SWCNTs and graphene with a high photoconductive gain $\sim 10^5$ [215]. The fabricated photodetector achieved a high responsivity of >100 A/W and a response time of ~ 100 μs (electrical bandwidth of $\sim 10^4$ Hz). The high built-in potential at the 1D and 2D interface provides efficient separation of photogenerated electron–hole pairs and decreases the recombination. Further, a fast response rate was achieved due to a trap-free interface. Lu and co-workers explored the implementation of a novel mechanism for exciton dissociation using graphene/MWCNT nanohybrids [216]. The fabricated photodetector was used for infrared detection and achieved high responsivity of ~ 3065 V/W and detectivity of 1.57×10^7 $\text{cm} \cdot \text{Hz}^{1/2}/\text{W}$.

7.4 Graphene-Based Photodetectors

Single-layer graphene has a wide-ranging but minimal absorption, due to this few-layer graphene was used to enhance the absorption. The other possibility to enhance the absorption in monolayer graphene was reported by Kang and co-workers for the first time [217]. They have used crumpled graphene which was intentionally deformed to get the continuous undulating 3D surface, to induce an increase in areal density that yields high optical absorption, hence improving the photoresponsivity. Mueller et al. reported graphene-based photodetector. In this asymmetric metal contacts and an interdigitated metal–graphene–metal was used on a Si/SiO₂ substrate [218]. The maximum responsivity of 6.1 mA/W was observed at 1550 nm. Liu et al. fabricated a photodetector using graphene double-layer heterostructure for ultra-broadband and high sensitivity of 4 A/W at room temperature. The device consists of two graphene layers sandwiching a thin SiO₂ barrier. The device consists of two graphene layers sandwiching a thin SiO₂ barrier.

7.5 Hybrid Photodetectors

Kim et al. reported a hybrid broadband photodetector based on carbon–carbon composite materials ranging from 300 nm (UV) to 1000 nm (NIR) wavelength, wherein GQDs were sandwiched between two graphene sheets (Fig. 21) [219]. SiO₂/Si was used as a substrate and two metal (silver) contacts were evaporated on top and bottom graphene layers. Although the design was symmetric, and asymmetric I–V characteristics were observed, which was ascribed to the charging or doping effects in the bottom layer of graphene. The fabricated device achieved the photoresponsivity of 0.5 A/W at 800 nm and the detectivity of 2.4×10^{11} Jones.

Sahatiya and co-workers reported a graphene/MoS₂ based visible light photodetector [220]. The internal electric field created due to graphene/MoS₂ heterostructure enhances the charge carriers separation which improves the responsivity of the photodetector. The same group demonstrated a flexible graphene-based infrared photodetector on PI substrate with responsivity and external quantum efficiency (EQE) of 0.4 A/W, 16.53%, respectively [120]. This project incorporates the synergistic advantages of the substrate (which acts as dielectric also) and sensing material. The same group optimized various parameters such as calcination temperature, time-dependent electrospinning of graphene/ZnO-based composite nanofiber across gold electrodes for UV detection which was fabricated by one-step in situ synthesis method [221]. The fabricated photodetector showed superior performance for UV sensing with an 1892 time increase in the conductance.

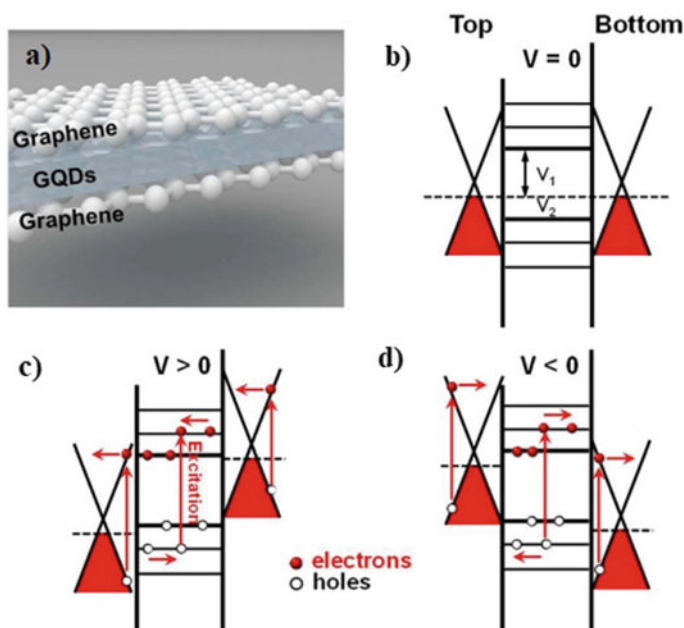


Fig. 21 Schematic illustration of band structure describing the photodetector **a** A typical GQD photodetector device and its band diagrams under **b** no, **c** positive (forward), and **d** negative (reverse) biases. Electrons and holes are represented by red and blank spots, respectively, and lateral arrows in the transport directions of holes and electrons contributing to dark- and photo-currents. Reprinted with permission from [219]. Copyright © 2014, Springer Nature

8 Conclusion and Outlook

It is apparent from above all sections in this chapter, carbon nanomaterials due to their unique thermal, mechanical, electronic properties have been proven to have the noteworthy potential to be used in various evolving electronic and sensing applications. Carbon nanomaterials which are available in different forms such as zero-dimensional (carbon quantum dots), one-dimensional (carbon nanotubes), two-dimensional (graphene), and their hybrids have shown significant impact in the fabrication of electronic and sensing devices. These fabricated devices helped in detecting various target analytes, dangerous gases, change in relative humidity/temperature/pressure, etc., and also increasing the non-volatile memory storage capacity by increasing the performance of fabricated electronic devices. Before realizing commercial carbon-based electronic and sensing devices for various applications, challenges must be addressed to avoid further complexities. Even though propels in development and post-manufactured partition strategies have significantly enhanced the carbon nanomaterials monodispersity, gadget-to-gadget inconstancy stays an issue. For instance, the threshold voltages of a variety of FETs created from semiconducting carbon nanotubes regularly differ by a few volts, which

is, at any rate, a significant degree higher than satisfactory in contemporary ICs. These dissimilarities can be mostly tended to by further upgrades in the faultlessness and monodispersity of the semiconducting carbon nanotubes bandgap, yet a significant part of the gadget inhomogeneity can likely be ascribed to extraneous factors, for example, the impact of metal contacts, dielectric layers, fundamental substrate, and general condition. Therefore, we predict that carbon nanomaterials will keep on being the subject of serious and productive exploration even as the first applications arrive at the commercial center.

Acknowledgments The authors acknowledge support from the Research Initiation Grant (RIG and ACRG), Birla Institute of Technology Pilani, Hyderabad Campus.

References

1. Kroto HW, McKay K (1988) The formation of quasi-icosahedral spiral shell carbon particles. *Nature* 331:328–331
2. Ugarte D (1992) Curling and closure of graphitic networks under electron-beam irradiation. *Nature* 359:707–709
3. Wang X, Hofmann O, Das R, Barrett EM, DeMello AJ, DeMello JC, Bradley DDC (2007) Integrated thin-film polymer/fullerene photodetectors for on-chip microfluidic chemiluminescence detection. *Lab Chip* 7:58–63
4. Deibel C, Dyakonov V (2010) Polymer–fullerene bulk heterojunction solar cells. *Mater Today* 73:462–470
5. Haddon RC, Perel AS, Morris RC, Palstra TTM, Hebard AF, Fleming RM (2012) C₆₀ thin film transistors. 121:1–4
6. Monthioux M, Kuznetsov VL (2006) Who should be given the credit for the discovery of carbon nanotubes? *Carbon N Y* 44:1621–1623
7. Radushkevich LV, Lukyanovich VM (1952) The structure of carbon forming in thermal decomposition of carbon monoxide on an iron catalyst. *Russ J Phys Chem* 26:88–95
8. Iijima S (1991) Helical microtubules of graphitic carbon. *Nature* 354:56–58
9. Inami N, Mohamed MA, Shikoh E, Fujiwara A (2007) Synthesis-condition dependence of carbon nanotube growth by alcohol catalytic chemical vapor deposition method. *Sci Technol Adv Mater* 8:292–295. <https://doi.org/10.1016/j.stam.2007.02.009>
10. Eftekhari A, Jafarkhani P, Moztarzadeh F (2006) High-yield synthesis of carbon nanotubes using a water-soluble catalyst support in catalytic chemical vapor deposition. *Carbon N Y* 44:1343–1345
11. Guo T, Nikolaev P, Rinzler AG, Tomanek D, Colbert DT, Smalley RE (1995) Self-assembly of tubular fullerenes. *J Phys Chem* 99:10694–10697
12. Ebbesen TW, Ajayan PM (1992) Large-scale synthesis of carbon nanotubes. *Nature* 358:220–222
13. Dai H (2002) Carbon nanotubes: opportunities and challenges. *Surf Sci* 500:218–241
14. Zhao X, Liu Y, Inoue S, Suzuki T, Jones RO, Ando Y (2004) Smallest carbon nanotube is 3 Å in diameter. *Phys Rev Lett* 92:125502
15. Wen Q, Zhang R, Qian W, Wang Y, Tan P, Nie J, Wei F (2010) Growing 20 cm long DWNTs/TWNTs at a rapid growth rate of 80–90 μm/s. *Chem Mater* 22:1294–1296
16. Dresselhaus EMS, Dresselhaus G, Avouris P (2003) Carbon nanotubes: synthesis, structure, properties, and applications. vol 80. Springer Science & Business Media
17. Reich S, Christian Thomsen JM (2004) Carbon nanotubes: basic concepts and physical properties

18. Ivchenko EL, Spivak B (2002) Chirality effects in carbon nanotubes. *Phys Rev B* 66:155404
19. Nakayama Y, Akita S (2001) Field-emission device with carbon nanotubes for a flat panel display. *Synth Met* 117:207–210
20. Varghese OK, Kichambre PD, Gong D, Ong KG, Dickey EC, Grimes CA (2001) Gas sensing characteristics of multi-wall carbon nanotubes. *Sensors Actuators B Chem* 81:32–41
21. Jiang W, Xiao S, Zhang H, Dong Y, Li X (2007) Capacitive humidity sensing properties of carbon nanotubes grown on silicon nanoporous pillar array. *Sci China Ser E Technol Sci* 50:510–515
22. Gao B, Kleinhammes A, Tang XP, Bower C, Fleming L, Wu Y, Zhou O (1999) Electrochemical intercalation of single-walled carbon nanotubes with lithium. *Chem Phys Lett* 307:153–157
23. Saha MS, Li R, Sun X, Ye S (2009) 3-D composite electrodes for high performance PEM fuel cells composed of Pt supported on nitrogen-doped carbon nanotubes grown on carbon paper. *Electrochem Commun* 11:438–441
24. Sun X, Li R, Villers D, Dodelet JP, Désilets S (2003) Composite electrodes made of Pt nanoparticles deposited on carbon nanotubes grown on fuel cell backings. *Chem Phys Lett* 379:99–104
25. Ghasempour R, Nareh H (2018) 1 - CNT Basics and characteristics. In: Rafiee RBT-CN-RP (ed) *Micro and Nano Technologies*. Elsevier, pp 1–24
26. Mashkoo F, Nasar A, Inamuddin, (2020) Carbon nanotube-based adsorbents for the removal of dyes from waters: a review. *Environ Chem Lett* 18:605–629
27. Messina G SS (2006) Carbon: the future material for advanced technology applications, p 530. Springer-Verlag Berlin Heidelberg
28. Morgan P (2005) Carbon fibers and their composites. Taylor & Francis Group, LLC, p P1200
29. Cheng H-Y, Zhu Y-A, Sui Z-J, Zhou X-G, Chen D (2012) Modeling of fishbone-type carbon nanofibers with cone-helix structures. *Carbon N Y* 50:4359–4372
30. Geim AK, Kim P (2008) Carbon wonderland. *Sci Am* 298:90–97
31. Novoselov KS, Geim AK, Morozov S V, Jiang D, Zhang Y, Dubonos SV, Grigorieva I V, Firsova AA (2004) Electric field effect in atomically thin carbon films. *Science* (80-) 306:666–669
32. Reina A, Jia X, Ho J, Nezich D, Son H, Bulovic V, Dresselhaus MS, Kong J (2009) Large area, few-layer graphene films on arbitrary substrates by chemical vapor deposition. *Nano Lett* 9:30–35
33. Dikin DA, Stankovich S, Zimney EJ, Piner RD, Dommett GHB, Evmenenko G, Nguyen ST, Ruoff RS (2007) Preparation and characterization of graphene oxide paper. *Nature* 448:457–460
34. Lotya M, Hernandez Y, King PJ, Smith RJ, Nicolosi V, Karlsson LS, Blighe FM, De S, Wang Z, McGovern IT, Duesberg GS, Coleman JN (2009) Liquid phase production of graphene by exfoliation of graphite in surfactant/water solutions. *J Am Chem Soc* 131:3611–3620
35. Geim AK, Novoselov KS (2007) The rise of graphene. *Nat Mater* 6:183–191
36. Lee C, Wei X, Kysar JW, Hone J (2008) Measurement of the elastic properties and intrinsic strength of monolayer graphene. *Science* (80-)321:385–388
37. Kuzmenko AB, van Heumen E, Carbone F, van der Marel D (2008) Universal optical conductance of graphite. *Phys Rev Lett* 100:117401
38. Balandin AA, Ghosh S, Bao W, Calizo I, Teweldebrhan D, Miao F, Lau CN (2008) Superior thermal conductivity of single-layer graphene. *Nano Lett* 8:902–907
39. Liu S, Chevali VS, Xu Z, Hui D, Wang H (2017) A review of extending performance of epoxy resins using carbon nanomaterials. *Compos Part B Eng* 136:197–214
40. Rizvi SB, Ghaderi S, Keshtgar M, Seifalian AM (2010) Semiconductor quantum dots as fluorescent probes for in vitro and in vivo bio-molecular and cellular imaging. *Nano Rev* 1:5161
41. Smith AM, Duan H, Mohs AM, Nie S (2008) Bioconjugated quantum dots for in vivo molecular and cellular imaging. *Adv Drug Deliv Rev* 60:1226–1240
42. Arya H, Kaul Z, Wadhwa R, Taira K, Hirano T, Kaul SC (2005) Quantum dots in bio-imaging: revolution by the small. *Biochem Biophys Res Commun* 329:1173–1177

43. Rizvi SB, Ghaderi S, Keshtgar M (2010) Semiconductor quantum dots as fluorescent probes for in vitro and in vivo bio-molecular and cellular imaging. *Nano Rev* 1(10):3402
44. Baker SN, Baker GA (2010) Luminescent carbon nanodots : emergent nanolights angewandte. *Angew Chem Int Ed* 49:6726–6744
45. Hu S-L, Niu K-Y, Sun J, Yang J, Zhao N-Q, Du X-W (2009) One-step synthesis of fluorescent carbon nanoparticles by laser irradiation. *J Mater Chem* 19:484–488
46. Ray SC, Saha A, Jana NR, Sarkar R (2009) Fluorescent carbon nanoparticles: synthesis, characterization, and bioimaging application. *J Phys Chem C* 113:18546–18551
47. Qiao Z-A, Wang Y, Gao Y, Li H, Dai T, Liu Y, Huo Q (2010) Commercially activated carbon as the source for producing multicolor photoluminescent carbon dots by chemical oxidation. *Chem Commun* 46:8812–8814
48. Zhou J, Booker C, Li R, Zhou X, Sham T-K, Sun X, Ding Z (2007) An electrochemical avenue to blue luminescent nanocrystals from multiwalled carbon nanotubes (MWCNTs). *J Am Chem Soc* 129:744–745
49. Bao L, Zhang Z-L, Tian Z-Q, Zhang L, Liu C, Lin Y, Qi B, Pang D-W (2011) Electrochemical tuning of luminescent carbon nanodots: from preparation to luminescence mechanism. *Adv Mater* 23:5801–5806
50. Sahatiya P, Jones SS, Badhulika S (2018) 2D MoS₂-carbon quantum dot hybrid based large area, flexible UV-vis-NIR photodetector on paper substrate. *Appl Mater Today* 10:106–114
51. Koduvayur Ganesan S, Selamneni V, Sahatiya P (2020) Water dissolvable MoS₂ quantum dots/PVA film as an active material for destructible memristors. *New J Chem*. <https://doi.org/10.1039/D0NJ02053B>
52. Jariwala D, Sangwan VK, Lauhon LJ, Marks TJ, Hersam MC (2013) Carbon nanomaterials for electronics, optoelectronics, photovoltaics, and sensing. *Chem Soc Rev* 42:2824–2860
53. Avouris P, Chen Z, Perebeinos V (2007) Carbon-Based Electronics. *Nat Nanotech* 2:605–615
54. Ando T, Nakanishi T (1998) Impurity scattering in carbon nanotubes—absence of back scattering. *J Phys Soc Japan* 67:1704–1713
55. Zhou X, Park J-Y, Huang S, Liu J, McEuen PL (2005) Band structure, phonon scattering, and the performance limit of single-walled carbon nanotube transistors. *Phys Rev Lett* 95:146805
56. Collins PG, Hersam M, Arnold M, Martel R, Avouris P (2001) Current saturation and electrical breakdown in multiwalled carbon nanotubes. *Phys Rev Lett* 86:3128–3131
57. Dürkop T, Getty SA, Cobas E, Fuhrer MS (2004) Extraordinary mobility in semiconducting carbon nanotubes. *Nano Lett* 4:35–39
58. Léonard F, Tersoff J (2000) Role of fermi-level pinning in nanotube schottky diodes. *Phys Rev Lett* 84:4693–4696
59. Chen Z, Appenzeller J, Knoch J, Lin Y (2005) The role of metal–nanotube contact in the performance of carbon nanotube field-effect transistors. *Nano Lett* 5:1–6
60. Sangwan VK, Ballarotto VW, Fuhrer MS, Williams ED, Sangwan VK, Ballarotto VW, Fuhrer MS, Williams ED (2014) Facile Fabrication of Suspended As-Grown Carbon Nanotube Devices. 93:113112
61. Franklin AD, Luisier M, Han S-J, Tulevski G, Breslin CM, Gignac L, Lundstrom MS, Haensch W (2012) Sub-10 nm carbon nanotube transistor. *Nano Lett* 12:758–762
62. Hickey BM, Oceanogr P, Emery WJ, Hamilton K, Res JG, Simpson JJ, Lett GR, Ely LL, Enzel Y, Cayan DR, Clim J, Prahl FG, Muehlhausen LA, Zahnle DL, Postma HWC, Teeppen T, Yao Z, Grifoni M (2001) Carbon nanotube single-electron transistors at room temperature. *Science* (80-) 293:76–79
63. Javey A, Guo J, Wang Q, Lundstrom M, Dai H (2003) Ballistic carbon nanotube field-effect transistors. *Nature* 424:654–657
64. Bockrath M, Cobden DH, Lu J (1999) Luttinger-liquid behaviour in carbon nanotubes. *Nature* 397:598–601
65. Martel R, Derycke V, Lavoie C, Appenzeller J, Chan KK, Tersoff J, Avouris P (2001) Ambipolar electrical transport in semiconducting single-wall carbon nanotubes. *Phys Rev Lett* 87:256805

66. Snow ES, Novak JP, Campbell PM, Park D, Snow ES, Novak JP, Campbell PM, Park D (2003) Random networks of carbon nanotubes as an electronic material. *Appl Phys Lett* 82:2145
67. Topinka MA, Rowell MW, Goldhaber-gordon D, McGehee MD, Hecht DS, Gruner G (2009) Charge transport in interpenetrating networks of semiconducting and metallic carbon nanotubes. *Nano Lett* 9:1866–1871
68. Collins PG, Arnold MS, Avouris P (2001) Engineering Carbon Nanotubes and Nanotube Circuits Using Electrical Breakdown. *Science* (80-) 292:706–709
69. Separated UH, Wang C, Zhang J, Zhou C (2010) Macroelectronic integrated circuits using high-performance separated carbon nanotube thin-film transistors. *ACS Nano* 4:7123–7132
70. Thin-film CN, Sangwan VK, Ortiz RP, Alaboson JMP, Emery JD, Bedzyk MJ, Lauhon LJ, Marks TJ, Hersam MC (2012) Fundamental performance limits of transistors achieved using hybrid molecular dielectrics. *ACS Nano* 6:7480–7488
71. Roberts ME, Lemieux MC, Sokolov AN, Bao Z (2009) Self-sorted nanotube networks on polymer dielectrics for low-voltage thin-film transistors. *Nano Lett* 9:2526–2531
72. Tans SJ, Verschueren ARM, Dekker C (1998) Room-temperature transistor based on a single carbon nanotube. *Nature* 393:49–52
73. Yao Z, Kane CL, Dekker C (2000) High-field electrical transport in single-wall carbon nanotubes. *Phys Rev Lett* 84:2941–2944
74. Steiner M, Engel M, Lin Y, Wu Y, Jenkins K, Farmer DB, Humes JJ, Yoder NL, Seo JT, Green AA, Hersam MC, Krupke R, Avouris P, Steiner M, Engel M, Lin Y, Wu Y, Jenkins K, Green AA, Hersam MC, Krupke R, Avouris P (2014) High-frequency performance of scaled carbon nanotube array field-effect transistors. *Appl Phys Lett* 101:053123
75. Cao Y, Brady GJ, Gui H, Rutherglen C, Arnold MS, Zhou C (2016) Radio frequency transistors using aligned semiconducting carbon nanotubes with current-gain cutoff frequency and maximum oscillation frequency simultaneously greater than 70 GHz. *ACS Nano* 10:6782–6790
76. Zhong D, Shi H, Ding L, Zhao C, Liu J, Zhou J, Zhang Z, Peng L (2019) Carbon nanotube film-based radio frequency transistors with maximum oscillation frequency above 100 GHz. *ACS Nano* 11:42496–42503
77. Raimond JM, Brune M, Computation Q, Martini F De, Monroe C (2004) Electric field effect in atomically thin carbon films. *Science* (80-) 306:666–669
78. Schwierz F (2010) Graphene transistors. *Nat Publ Gr* 5:487–496
79. Neto AHC (2009) The electronic properties of graphene. *RevModPhys* 81:109–162
80. Lin Y, Dimitrakopoulos C, Jenkins KA, Farmer DB, Chiu H, Grill A, Avouris P (2010) 100-GHz transistors from wafer-scale epitaxial graphene. *Science* (80-) 327:662
81. Badmaev A, Che Y, Li Z, Wang C, Zhou C (2012) Self-aligned fabrication of graphene RF transistors with T-shaped gate. *ACS Nano* 6:3371–3376
82. Guo Z, Dong R, Chakraborty PS, Lourenco N, Palmer J, Hu Y, Ruan M, Hankinson J, Kunc J, Cressler JD, Berger C, De HWA (2013) Record maximum oscillation frequency in C-face epitaxial graphene transistors. *Nano Lett* 13:942–947
83. Sur UK (2012) Graphene: a rising star on the horizon of materials science. *Int J Electrochem* 2012:237689
84. Khan K, Tareen AK, Aslam M, Wang R, Zhang Y, Mahmood A, Ouyang Z, Zhang H, Guo Z (2020) Recent developments in emerging two-dimensional materials and their applications. *J Mater Chem C* 8:387–440
85. Kalavakunda V, Hosmane NS (2016) Mini review graphene and its analogues. *Nanotechnol Rev* 5:369–376
86. Kim K, Choi J, Kim T, Cho S, Chung H (2011) A role for graphene in silicon-based semiconductor devices. *Nature* 479:338–344
87. Feng X, Zhao X, Yang L, Li M, Qie F, Guo J, Zhang Y, Li T (2018) All carbon materials pn diode. *Nat Commun* 9:3750
88. Jariwala D, Sangwan VK, Wu C, Prabhurashi PL, Geier ML (2013) Gate-tunable carbon nanotube–MoS₂ heterojunction p-n diode. *PNAS* 110:18076–18080

89. Yang Y, Zhao Q, Feng W, Li F (2013) Luminescent chemodosimeters for bioimaging. *ChemRev* 113:192–270
90. Fan Q, Li J, Zhu Y, Yang Z, Shen T, Guo Y, Wang L, Mei T, Wang J, Wang X (2020) Functional carbon quantum dots for highly sensitive graphene transistors for Cu²⁺ ion detection. *ACS Appl Mater Interfaces* 12:4797–4803
91. Liu W, Song M, Kong B, Cui Y (2017) Flexible and stretchable energy storage: recent advances and future perspectives. *Adv Mater* 29:1603436
92. Khang D-Y, Jiang H, Huang Y, Rogers JA (2006) A stretchable form of single-crystal silicon for high-performance electronics on rubber substrates. *Science* (80-) 311:208 LP–212
93. Nanotube GC, Huang J, Fang J, Liu C, Chu C (2011) Effective work function modulation of graphene/carbon nanotube composite films as transparent cathodes for organic optoelectronics. *ACS Nano* 5:6262–6271
94. Cao Q, Hur S-H, Zhu Z-T, Sun YG, Wang C-J, Meitl MA, Shim M, Rogers JA (2006) Highly bendable, transparent thin-film transistors that use carbon-nanotube-based conductors and semiconductors with elastomeric dielectrics. *Adv Mater* 18:304–309
95. Aikawa S Transparent all-carbon-nanotube transistors D transparent all-carbon-nanotube transistors, Einarsson E, Thurakitseree T, Chiashi S, Nishikawa E (2012) Deformable transparent all-carbon-nanotube transistors. *Appl Phys Lett* 100:063502
96. Sun D, Timmermans MY, Tian Y, Nasibulin AG, Kauppinen EI, Kishimoto S, Mizutani T, Ohno Y (2011) Flexible high-performance carbon nanotube integrated circuits. *Nat Nanotech* 6:156–161
97. Sun D, Timmermans MY, Kaskela A, Nasibulin AG, Kishimoto S, Mizutani T, Kauppinen EI, Ohno Y (2013) Mouldable all-carbon integrated circuits. *Nat Commun* 4:2302
98. Lu R, Christianson C, Weintrub B, Wu JZ (2013) High photoresponse in hybrid graphene–carbon nanotube infrared detectors. *ACS Appl Mater Interfaces* 5:11703–11707
99. Kim SH, Song W, Jung MW, Kang M, Kim K (2014) Carbon nanotube and graphene hybrid thin film for transparent electrodes and field effect transistors. *Adv Mater* 26:4247–4252
100. Tung VC, Chen L, Allen MJ, Wassei JK, Nelson K, Kaner RB, Yang Y (2009) Low-temperature solution processing of graphene-carbon nanotube hybrid materials for high-performance transparent conductors. *Nano Lett* 9:1949–1955
101. Yakobson BI, Brabec CJ, Bernholc J (1996) Nanomechanics of carbon tubes: instabilities beyond linear response. *Phys Rev Lett* 76:2511–2514
102. Wong EW, Sheehan PE, Lieber CM (1997) Nanobeam mechanics: elasticity, strength, and toughness of nanorods and nanotubes. *Science* (80-) 277:1971–1975
103. Selamneni V, Barya P, Deshpande N, Sahatiya P (2019) Low-cost, disposable, flexible, and smartphone enabled pressure sensor for monitoring drug dosage in smart medicine applications. *IEEE Sens J* 19:11255–11261
104. Selamneni V, Dave A, Mihailovic P, Mondal S, Sahatiya P (2020) Large area pressure sensor for smart floor sensor applications—an occupancy limiting technology to combat social distancing. *IEEE Consum Electron Mag*. <https://doi.org/10.1109/MCE.2020.3033932>
105. Selamneni V, Dave A, Mihailovic P, Mondal S and Sahatiya P (2020) Large area pressure sensor for smart floor sensor applications—an occupancy limiting technology to combat social distancing. *IEEE Consum Electron Mag*. <https://doi.org/10.1109/MCE.2020.3033932>.
106. Selamneni V, B S A, Sahatiya P(2020) Highly air-stabilized black phosphorus on disposable paper substrate as a tunnelling effect-based highly sensitive piezoresistive strain sensor. *Med Dev Sensors* 3:e10099
107. Zhan Z, Lin R, Tran V, An J, Wei Y, Du H, Tran T, Lu W (2017) Paper/carbon nanotube-based wearable pressure sensor for physiological signal acquisition and soft robotic skin. *ACS Appl Mater Interfaces* 9:37921–37928
108. Sahatiya P, Badhulika S (2016) Solvent-free fabrication of multi-walled carbon nanotube based flexible pressure sensors for ultra-sensitive touch pad and electronic skin applications. *RSC Adv* 6:95836–95845
109. Park J, Kim M, Lee Y, Lee HS, Ko H (2015) Fingertip skin-inspired microstructured ferroelectric skins discriminate static / dynamic pressure and temperature stimuli. *Sci Adv* 1:e1500661

110. Zhu S, Ghatkesar MK, Zhang C, Janssen GCAM, Zhu S, Ghatkesar K, Zhang C, Janssen GCAM (2013) Graphene based piezoresistive pressure sensor. *Appl Phys Lett* 102:161904
111. Yao H, Ge J, Wang C, Wang X, Hu W, Zheng Z (2013) A flexible and highly pressure-sensitive graphene-polyurethane sponge based on fractured microstructure design. *Adv Mater* 25:6692–6698
112. Jian M, Xia K, Wang Q, Yin Z, Wang H, Wang C (2017) Flexible and highly sensitive pressure sensors based on bionic hierarchical structures. *RSC Adv* 9:22740–22748
113. Tian H, Shu Y, Wang X, Mohammad MA, Bie Z, Xie Q, Li C, Mi W, Yang Y, Ren T (2015) A graphene-based resistive pressure sensor with record-high sensitivity in a wide pressure range. *Sci Rep* 5:8603
114. Lee MJ, Hong HP, Min NK, Lee D (2012) A fully-microfabricated SWCNT film strain sensor. *J Korean Phys Soc* 61:1656–1659
115. Dharap P, Li Z, Nagarajaiah S (2004) Nanotube film based on single-wall carbon nanotubes for strain sensing. *Nanotechnology* 15:379–382
116. Zhang S, Zhang H, Yao G, Liao F, Gao M, Huang Z, Li K, Lin Y (2015) Highly stretchable, sensitive, and flexible strain sensors based on silver nanoparticles/carbon nanotubes composites. *J Alloys Compd* 652:48–54
117. Zhao J, He C, Yang R, Shi Z, Cheng M, Yang W, Xie G, Wang D, Shi D, Zhang G (2012) Ultra-sensitive strain sensors based on piezoresistive nanographene films. *Appl Phys Lett* 101:63112
118. Li X, Zhang R, Yu W, Wang K, Wei J, Wu D, Cao A, Li Z, Cheng Y, Zheng Q, Ruoff RS, Zhu H (2012) Stretchable and highly sensitive graphene-on-polymer strain sensors. *Sci Rep* 2:870
119. Davaji B, Cho HD, Malakoutian M, Lee J, Panin G, Kang TW, Lee CH (2017) A patterned single layer graphene resistance temperature sensor. *Sci Rep* 7:8811
120. Sahatiya P, Puttapati SK, Srikanth VVSS, Badhulika S (2016) Graphene-based wearable temperature sensor and infrared photodetector on a flexible polyimide substrate. *Flex Print Electron* 1:25006
121. Compagnone D, Di Francia G, Di Natale C, Neri G, Seeber R, Tajani A (2017) Chemical sensors and biosensors in Italy: a review of the 2015 literature. *Sensors (Switzerland)* 17:1–22
122. Veeralingam S, Sahatiya P, Badhulika S (2019) Low cost, flexible and disposable SnSe₂ based photoresponsive ammonia sensor for detection of ammonia in urine samples. *Sens Actuators B Chem* 297:126725
123. Bokka N, Selamneni V, Sahatiya P (2020) A water destructible SnS₂ QD/PVA film based transient multifunctional sensor and machine learning assisted stimulus identification for non-invasive personal care diagnostics. *Mater Adv*. <https://doi.org/10.1039/d0ma00573h>
124. Selamneni V, Gohel K, Bokka N, Sharma S, Sahatiya P (2020) MoS₂ based Multifunctional sensor for both chemical and physical stimuli and their classification using machine learning algorithms. *IEEE Sens J*. <https://doi.org/10.1109/JSEN.2020.3023309>
125. Leelasree T, Selamneni V, Akshaya T, Sahatiya P, Aggarwal H (2020) MOF based flexible, low-cost chemiresistive device as a respiration sensor for sleep apnea diagnosis. *J Mater Chem B*. <https://doi.org/10.1039/D0TB01748E>
126. Sahatiya P, Badhulika S (2016) Graphene hybrid architectures for chemical sensors. Springer, Cham, Switzerland, pp 259–285
127. Yang S, Jiang C, Wei SH (2017) Gas sensing in 2D materials. *Appl Phys Rev* 4:021304
128. Fine GF, Cavanagh LM, Afonja A, Binions R (2010) Metal oxide semi-conductor gas sensors in environmental monitoring. *Sensors* 10:5469–5502
129. Zhang J, Liu X, Neri G, Pinna N (2016) Nanostructured materials for room-temperature gas sensors. *Adv Mater* 28:795–831
130. Choi S-J, Jang B-H, Lee S-J, Min BK, Rothschild A, Kim I-D (2014) Selective detection of acetone and hydrogen sulfide for the diagnosis of diabetes and halitosis using SnO₂ nanofibers functionalized with reduced graphene oxide nanosheets. *ACS Appl Mater Interfaces* 6:2588–2597

131. Li W, Geng X, Guo Y, Rong J, Gong Y, Wu L, Zhang X, Li P, Xu J, Cheng G, Sun M, Liu L (2011) Reduced graphene oxide electrically contacted graphene sensor for highly sensitive nitric oxide detection. *ACS Nano* 5:6955–6961
132. Schedin F, Geim AK, Morozov SV, Hill EW, Blake P, Katsnelson MI, Novoselov KS (2007) Detection of individual gas molecules adsorbed on graphene. *Nat Mater* 6:652–655
133. Dan Y, Lu Y, Kybert NJ, Luo Z, Johnson ATC (2009) Intrinsic response of graphene vapor sensors. *Nano Lett* 9:1472–1475
134. Rumyantsev S, Liu G, Shur MS, Potyrailo RA, Balandin AA (2012) Selective gas sensing with a single pristine graphene transistor. *Nano Lett* 12:2294–2298
135. Gautam M, Jayatissa AH (2012) Detection of organic vapors by graphene films functionalized with metallic nanoparticles. *J Appl Phys* 112:114326
136. Yavari F, Chen Z, Thomas AV, Ren W, Cheng H-M, Koratkar N (2011) High sensitivity gas detection using a macroscopic three-dimensional graphene foam network. *Sci Rep* 1:166
137. Kumar S, Kaushik S, Pratap R, Raghavan S (2015) Graphene on paper: a simple, low-cost chemical sensing platform. *ACS Appl Mater Interfaces* 7:2189–2194
138. Park S, Park M, Kim S, Yi S, Kim M, Son J, Cha J, Hong J, Park S, Park M, Kim S, Yi S, Kim M, Son J (2017) NO₂ gas sensor based on hydrogenated graphene. *Appl Phys Lett* 111:213102
139. Kim YH, Kim SJ, Kim Y-J, Shim Y-S, Kim SY, Hong BH, Jang HW (2015) Self-activated transparent all-graphene gas sensor with endurance to humidity and mechanical bending. *ACS Nano* 9:10453–10460
140. Choi H, Choi JS, Kim J-S, Choe J-H, Chung KH, Shin J-W, Kim JT, Youn D-H, Kim K-C, Lee J-I, Choi S-Y, Kim P, Choi C-G, Yu Y-J (2014) Flexible and transparent gas molecule sensor integrated with sensing and heating graphene layers. *Small* 10:3685–3691
141. Robinson JT, Perkins FK, Snow ES, Wei Z, Sheehan PE (2008) Reduced graphene oxide molecular sensors. *Nano Lett* 8:3137–3140
142. Dua V, Surwade SP, Ammu S, Agnihotra SR, Jain S, Roberts KE, Park S, Ruoff RS, Manohar SK (2010) All-organic vapor sensor using inkjet-printed reduced graphene oxide. *Angew Chemie Int Ed* 49:2154–2157
143. Chung MG, Kim DH, Seo DK, Kim T, Im HU, Lee HM, Yoo JB, Hong SH, Kang TJ, Kim YH (2012) Flexible hydrogen sensors using graphene with palladium nanoparticle decoration. *Sens Actuators B Chem* 169:387–392
144. Khalaf AL, Mohamad FS, Rahman NA, Lim HN, Paiman S, Yusof NA, Mahdi MA, Yaacob MH (2017) Room temperature ammonia sensor using side-polished optical fiber coated with graphene/polyaniline nanocomposite. *Opt Mater Express* 7:1858–1870
145. Deng S, Tjoa V, Fan HM, Tan HR, Sayle DC, Olivo M, Mhaisalkar S, Wei J, Sow CH (2012) Reduced Graphene oxide conjugated Cu₂O nanowire mesocrystals for high-performance NO₂ gas sensor. *J Am Chem Soc* 134:4905–4917
146. Al-Mashat L, Shin K, Kalantar-zadeh K, Plessis JD, Han SH, Kojima RW, Kaner RB, Li D, Gou X, Ippolito SJ, Wlodarski W (2010) Graphene/polyaniline nanocomposite for hydrogen sensing. *J Phys Chem C* 114:16168–16173
147. Jeong HY, Lee DS, Choi HK, Lee DH, Kim JE, Lee JY, Lee WJ, Kim SO, Choi SY (2010) Flexible room-temperature NO₂ gas sensors based on carbon nanotubes/reduced graphene hybrid films. *Appl Phys Lett* 96:2010–2013
148. Yang W, Wan P, Zhou X, Hu J, Guan Y, Feng L (2014) Additive-Free Synthesis Of In₂O₃ cubes embedded into graphene sheets and their enhanced NO₂ sensing performance at room temperature. *ACS Appl Mater Interfaces* 6:21093–21100
149. Zhang D, Chang H, Li P, Liu R (2016) Characterization of nickel oxide decorated-reduced graphene oxide nanocomposite and its sensing properties toward methane gas detection. *J Mater Sci Mater Electron* 27:3723–3730
150. Kraus F, Cruz S, Müller J (2003) Plasmopolymerized silicon organic thin films from HMDSN for capacitive humidity sensors. *Sens Actuators B Chem* 88:300–311
151. Rittersma ZM (2002) Recent achievements in miniaturised humidity sensors-a review of transduction techniques. *Sensors Actuators* 96:196–210

152. Varghese OK, Grimes CA (2003) Metal oxide nanoarchitectures for environmental sensing. *J Nanosci Nanotechnol* 3:277–293
153. Rittersma ZM, Splinter A, Bodecker A, Benecke W (2000) A novel surface-micromachined capacitive porous silicon humidity sensor. *Sens Actuators B* 68:210–217
154. Björkqvist M, Salonen J, Paski J, Laine E (2004) Characterization of thermally carbonized porous silicon humidity sensor. *Sens Actuators a Phys* 112:244–247
155. Chu J, Peng X, Feng P, Sheng Y, Zhang J (2013) Sensors and actuators B: chemical Study of humidity sensors based on nanostructured carbon films produced by physical vapor deposition. *Sens Actuators B Chem* 178:508–513
156. Jin H, Tao X, Feng B, Yu L, Wang D, Dong S (2017) A humidity sensor based on quartz crystal microbalance using graphene oxide as a sensitive layer. *Vacuum* 140:101–105
157. Kumar U, Yadav BC (2019) Development of humidity sensor using modified curved MWCNT based thin film with DFT calculations. *Sens Actuators B Chem* 288:399–407
158. Borini S, White R, Wei D, Astley M, Haque S, Spigone E, Harris N (2013) Ultrafast graphene oxide humidity sensors. *ACS Nano* 7:11166–11173
159. Dresselhaus BMS, Terrones M (2013) Carbon-based nanomaterials from a historical perspective. *Proc IEEE* 101:1522–1535
160. Wang Y, Huang K, Wu X (2017) Recent advances in transition-metal dichalcogenides based electrochemical biosensors: a review. *Biosens Bioelectron* 97:305–316
161. Arvizo RR, Bhattacharyya S, Kudgus RA, Giri K, Bhattacharya RMP (2012) Intrinsic therapeutic applications of noble metal nanoparticles: past, present and future. *Chem Soc Rev* 41:2943–2970
162. Kwon SJ, Bard AJ (2012) DNA analysis by application of Pt nanoparticle electrochemical amplification with single label response. *J Am Chem Soc* 134:10777–10779
163. Wu S, He Q, Tan C, Wang Y, Zhang H (2013) Graphene-based electrochemical sensors. *Small* 9:1160–1172
164. Kochmann S, Hirsch T, Wolfbeis OS (2012) Graphenes in chemical sensors and biosensors. *TrAC Trends Anal Chem* 39:87–113
165. Balasubramanian RK, Burghard M (2006) Biosensors based on carbon nanotubes. *Anal Bioanal Chem* 385:452–468
166. Wang J, Lin Y (2008) Functionalized carbon nanotubes and nanofibers for biosensing applications. *Trends Analyt Chem* 27:619–626
167. Griese S, Kampouris DK, Kadara RO, Banks CE (2008) A critical review of the electrocatalysis reported at C₆₀ modified electrodes. *Electroanalysis* 20:1507–1512
168. Tang X, Liu Y, Hou H, You T (2010) Electrochemical determination of L -Tryptophan, L -Tyrosine and L-Cysteine using electrospun carbon nanofibers modified electrode. *Talanta* 80:2182–2186
169. Nguyen HV, Richtera L, Moullick A, Xhaxhiu K, Kudr J, Cernei N, Polanska H, Heger Z, Masarik M, Kopel P, Stiborova M, Eckschlager T, Adam V, Kizek R (2016) Electrochemical sensing of etoposide using carbon quantum dot modified glassy carbon electrode. *Analyst* 141:2665–2675
170. Santhanam KSV, Ajayan PM (1996) Carbon nanotube electrode for oxidation of dopamine. *Bioelectrochemistry Bioenerg* 41:121–125
171. Luo H, Shi Z, Li N, Gu Z, Zhuang Q (2001) Investigation of the electrochemical and electrocatalytic behavior of single-wall carbon nanotube film on a glassy carbon electrode. *Anal Chem* 73:915–920
172. Joshi KA, Tang J, Haddon R, Wang J, Chen W, Mulchandani A (2005) A disposable biosensor for organophosphorus nerve agents based on carbon nanotubes modified thick film strip electrode. *Electroanalysis* 17:54–58
173. Lefrant S, Baibarac M, Baltog I, Mevellec JY, Mihut L, Chauvet O (2004) SERS spectroscopy studies on the electrochemical oxidation of single-walled carbon nanotubes in sulfuric acid solutions. *Synth Met* 144:133–142
174. Rakhi RB, Sethupathi K, Ramaprabhu S (2009) A Glucose biosensor based on deposition of glucose oxidase onto crystalline gold nanoparticle modified carbon nanotube electrode. *J Phys Chem B* 113:3190–3194

175. Qiu J-D, Huang J, Liang R-P (2011) Nanocomposite film based on graphene oxide for high performance flexible glucose biosensor. *Sens Actuators B Chem* 160:287–294
176. Lu W, Luo Y, Chang G, Sun X (2011) Synthesis of functional SiO₂-coated graphene oxide nanosheets decorated with Ag nanoparticles for H₂O₂ and glucose detection. *Biosens Bioelectron* 26:4791–4797
177. Shan C, Yang H, Han D, Zhang Q, Ivaska A, Niu L (2010) Graphene/AuNPs/chitosan nanocomposites film for glucose biosensing. *Biosens Bioelectron* 25:1070–1074
178. Liu Y, Yu D, Zeng C, Miao Z, Dai L (2010) Biocompatible graphene oxide-based glucose biosensors. *Langmuir* 26:6158–6160
179. Wu P, Shao Q, Hu Y, Jin J, Yin Y, Zhang H, Cai C (2010) Direct electrochemistry of glucose oxidase assembled on graphene and application to glucose detection. *Electrochim Acta* 55:8606–8614
180. Chen Y, Li Y, Sun D, Tian D, Zhang J, Zhu J-J (2011) Fabrication of gold nanoparticles on bilayer graphene for glucose electrochemical biosensing. *J Mater Chem* 21:7604–7611
181. Wang K, Liu Q, Guan Q-M, Wu J, Li H-N, Yan J-J (2011) Enhanced direct electrochemistry of glucose oxidase and biosensing for glucose via synergy effect of graphene and CdS nanocrystals. *Biosens Bioelectron* 26:2252–2257
182. Sun J-Y, Huang K-J, Fan Y, Wu Z-W, Li D-D (2011) Glassy carbon electrode modified with a film composed of Ni(II), quercetin and graphene for enzyme-less sensing of glucose. *Microchim Acta* 174:289
183. Lee J-S (2011) Progress in non-volatile memory devices based on nanostructured materials and nanofabrication. *J Mater Chem* 21:14097–14112
184. Sawa A (2008) Resistive switching in transition metal oxides. *Mater Today* 11:28–36
185. Waser R, Aono M (2007) Nanoionics-based resistive switching memories. *Nat Mater* 6:833–840
186. Lee M, Han S, Jeon SH, Park BH, Kang BS, Ahn S, Kim KH, Lee CB, Kim CJ, Yoo I, Seo DH, Li X, Park J, Lee J, Park Y (2009) Electrical manipulation of nanofilaments in transition-metal oxides for resistance-based memory. *Nano Lett* 9:1476–1481
187. Waser R, Dittmann R, Staikov G, Szot K (2009) Redox-based resistive switching memories—nanoionic mechanisms, prospects, and challenges. *Adv Mater* 21:2632–2663
188. Watanabe Y, Bednorz JG, Bietsch A, Gerber C, Widmer D, Beck A, Wind SJ, Watanabe Y, Bednorz JG, Bietsch A, Gerber C, Widmer D, Beck A (2001) Current-driven insulator–conductor transition and nonvolatile memory in chromium-doped SrTiO₃ single crystals. *Appl Phys Lett* 78:3738
189. Seo S, Lee MJ, Seo DH, Jeoung EJ, Suh D, Seo S, Lee MJ, Seo DH, Jeoung EJ, Suh D, Jeoung YS, Yoo IK (2004) Reproducible resistance switching in polycrystalline NiO films. *Appl Phys Lett* 85:5655
190. Beck A, Bednorz JG, Gerber C, Rossel C, Widmer D, Beck A, Bednorz JG, Gerber C, Rossel C, Widmer D (2000) Reproducible switching effect in thin oxide films for memory applications. *Appl Phys Lett* 77:139
191. Rani A and Kim D.H. (2016) A mechanistic study on graphene-based nonvolatile ReRAM devices. *J Mater Chem C* 4:11007–11031
192. Hlee Ā, Hen PC, Ang CW, Aikap SM (2007) Low-Power Switching of nonvolatile resistive memory using hafnium oxide low-power switching of nonvolatile resistive memory using hafnium oxide. *Jpn J Appl Phys* 46:2175–2179
193. Yalagala B, Sahatiya P, Mattela V, Badhulika S (2019) Ultra-low cost, large area graphene/MoS₂-based piezotronic memristor on paper: a systematic study for both direct current and alternating current inputs. *ACS Appl Electron Mater* 1:883–891
194. Tsai C, Xiong F, Pop E, Shim M, Science M, Seitz F, Engineering C, States U (2013) Resistive random access memory enabled by carbon nanotube. *ACS Nano* 7:5360–5366
195. Yang P, Chang W, Teng P, Jeng S, Lin S, Chiu P, He J (2013) Fully transparent resistive memory employing graphene electrodes for eliminating undesired surface effects. *Proc IEEE* 101:1732–1739

196. Selamneni V, Nerurkar N, Sahatiya P (2020) Large area deposition of MoSe₂ on paper as a flexible near-infrared photodetector. *IEEE Sens Lett* 4:1–4
197. Sahatiya P, Solomon Jones S, Thanga Gomathi P, Badhulika S (2017) Flexible substrate based 2D ZnO (n)/graphene (p) rectifying junction as enhanced broadband photodetector using strain modulation. *2D Mater* 4:25053
198. Veerla RS, Sahatiya P, Badhulika S (2017) Fabrication of a flexible UV photodetector and disposable photoresponsive uric acid sensor by direct writing of ZnO pencil on paper. *J Mater Chem C* 5:10231–10240
199. Selamneni V, Koduvayur Ganeshan S, Sahatiya P (2020) All MoS₂ based 2D/0D localized unipolar heterojunctions as a flexible broadband (UV-Vis-NIR) photodetector. *J Mater Chem C*. <https://doi.org/10.1039/D0TC02651D>
200. Yang D, Ma D (2019) Development of organic semiconductor photodetectors: from mechanism to applications. *Adv Opt Mater* 7:1800522
201. Selamneni V, Sahatiya P (2020) Bolometric effect enhanced ultrafast graphene based do-it-yourself wearable respiration sensor for personal healthcare monitoring. *IEEE Sens J* 20:3452–3459
202. Sahatiya P, Badhulika S (2017) Strain-modulation-assisted enhanced broadband photodetector based on large-area, flexible, few-layered Gr/MoS₂ on cellulose paper. *Nanotechnology* 28:455204
203. Joshna P, Gollu SR, Raj PMP, Rao BVVSNP, Sahatiya P, Kundu S (2019) Plasmonic Ag nanoparticles arbitrated enhanced photodetection in p-NiO/n-rGO heterojunction for future self-powered UV photodetectors. *Nanotechnology* 30:365201
204. Sahatiya P, Shinde A, Badhulika S (2018) Pyro-phototronic nanogenerator based on flexible 2D ZnO/graphene heterojunction and its application in self-powered near infrared photodetector and active analog frequency modulation. *Nanotechnology* 29:325205
205. Sahatiya P, Badhulika S (2016) UV/ozone assisted local graphene (p)/ZnO(n) heterojunctions as a nanodiode rectifier. *J Phys D Appl Phys* 49:265101
206. Sahatiya P, Gopalakrishnan A, Badhulika S (2017) Paper based large area Graphene/MoS₂ visible light photodetector. In: 2017 IEEE 17th International Conference on Nanotechnology (IEEE-NANO), pp 728–730
207. Ma L, Ouyang J, Yang Y (2004) High-speed and high-current density C60 diodes. *Appl Phys Lett* 84:4786–4788
208. Szendrei K, Cordella F, Kovalenko MV, Böberl M, Hesser G, Yarema M, Jarzab D, Mikhnenko OV, Gocalinska A, Saba M, Quochi F, Mura A, Bongiovanni G, Blom PWM, Heiss W, Loi MA (2009) Solution-Processable near-IR photodetectors based on electron transfer from PbS nanocrystals to fullerene derivatives. *Adv Mater* 21:683–687
209. Guo F, Xiao Z, Huang J (2013) Photodetectors: fullerene photodetectors with a linear dynamic range of 90 dB enabled by a cross-linkable buffer layer (*Advanced Optical Materials* 4/2013). *Adv Opt Mater* 1:275
210. Zhang Q, Jie J, Diao S, Shao Z, Zhang Q, Wang L, Deng W, Hu W, Xia H, Yuan X, Lee S-T (2015) Solution-processed graphene quantum dot deep-UV photodetectors. *ACS Nano* 9:1561–1570
211. Tang L, Ji R, Li X, Bai G, Liu CP, Hao J, Lin J, Jiang H, Teng KS, Yang Z, Lau SP (2014) Deep ultraviolet to near-infrared emission and photoresponse in layered N-doped graphene quantum dots. *ACS Nano* 8:6312–6320
212. Rao F, Liu X, Li T, Zhou Y, Wang Y (2009) The synthesis and fabrication of horizontally aligned single-walled carbon nanotubes suspended across wide trenches for infrared detecting application. *Nanotechnology* 20:55501
213. Liu Y, Wei N, Zeng Q, Han J, Huang H, Zhong D, Wang F, Ding L, Xia J, Xu H, Ma Z, Qiu S, Li Q, Liang X, Zhang Z, Wang S, Peng L-M (2016) Room temperature broadband infrared carbon nanotube photodetector with high detectivity and stability. *Adv Opt Mater* 4:238–245
214. He X, Fujimura N, Lloyd JM, Erickson KJ, Talin AA, Zhang Q, Gao W, Jiang Q, Kawano Y, Hauge RH, Léonard F, Kono J (2014) Carbon nanotube terahertz detector. *Nano Lett* 14:3953–3958

215. Liu Y, Wang F, Wang X, Wang X, Flahaut E, Liu X, Li Y, Wang X, Xu Y, Shi Y, Zhang R (2015) Planar carbon nanotube–graphene hybrid films for high-performance broadband photodetectors. *Nat Commun* 6:8589
216. Lu R, Christianson C, Weintrub B, Wu JZ (2013) High photoresponse in hybrid graphene–carbon nanotube infrared detectors. *ACS Appl Mater Interfaces* 5:11703–11707
217. Kang P, Wang MC, Knapp PM, Nam S (2016) Crumpled graphene photodetector with enhanced, strain-tunable, and wavelength-selective photoresponsivity. *Adv Mater* 28:4639–4645
218. Mueller T, Xia F, Avouris P (2010) Graphene photodetectors for high-speed optical communications. *Nat Photonics* 4:297–301
219. Kim CO, Hwang SW, Kim S, Shin DH, Kang SS, Kim JM, Jang CW, Kim JH, Lee KW, Choi S-H, Hwang E (2014) High-performance graphene-quantum-dot photodetectors. *Sci Rep* 4:5603
220. Gomathi PT, Sahatiya P, Badhulika S (2017) Large-area, flexible broadband photodetector based on ZnS–MoS₂ hybrid on paper substrate. *Adv Funct Mater* 27:1701611
221. Sahatiya P, Badhulika S (2015) One-step in situ synthesis of single aligned graphene–ZnO nanofiber for UV sensing. *RSC Adv* 5:82481–82487